Development of High-Fidelity Structural Finite Element Analysis and Optimization Capability for Aeroelastic Applications

Evan Anderson

PhD Defense

Department of Mechanical Engineering

August 28, 2019

University of Wyoming

Outline

I. Background & Motivation
   a) Need for high-fidelity simulations in aerodynamics & aeroelastic analysis
   b) The adjoint, and optimization in aero-structural dynamics
   c) Past and present work in UW CFD lab
II. AStrO: Adjoint-Based Structural Optimizer
   a) Fundamental FEA formulation of structural thermoelastic modeling
   b) Fluid-structure interface for coupling with CFD codes
   c) Formulation of the discrete adjoint for structural thermoelastic equations
III. Demonstrations & Validations
   a) Validation of static thermoelastic modeling & sensitivities
   b) Validation of dynamic modeling
   c) Validation of coupled aero-structural modeling
IV. Case Studies
   I. Fatigue stress minimization on SWiFT Wind turbine blade
   II. Investigations of methods for application of buckling constraints
V. Conclusions

High-Fidelity Simulations

In computational aerodynamics, high fidelity simulations are generally required for meaningful results

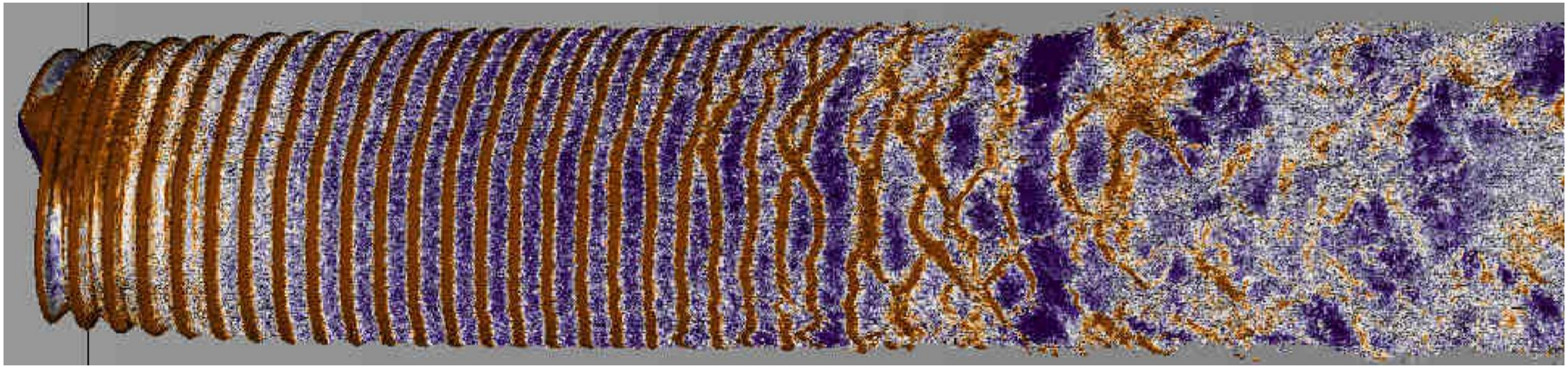

*Kirby et al. (2018)

Optimization methods with minimal flow solutions are desirable

*Kirby, A., Yang, Z., and Mavriplis, D., “Visualization and Data Analytics Challenges of Large-Scale High-Fidelity Numerical Simulations of Wind Energy Applications,” *2018 AIAA Aerospace Sciences Meeting,* CP18-1171, 2018.

Gradient-Based Optimization

Gradient optimization is generally suitable for aerodynamic/aero-structural applications, where the objective is a smooth function of many design variables

Objective $= L\big(D_i, U_j(D_i)\big)$

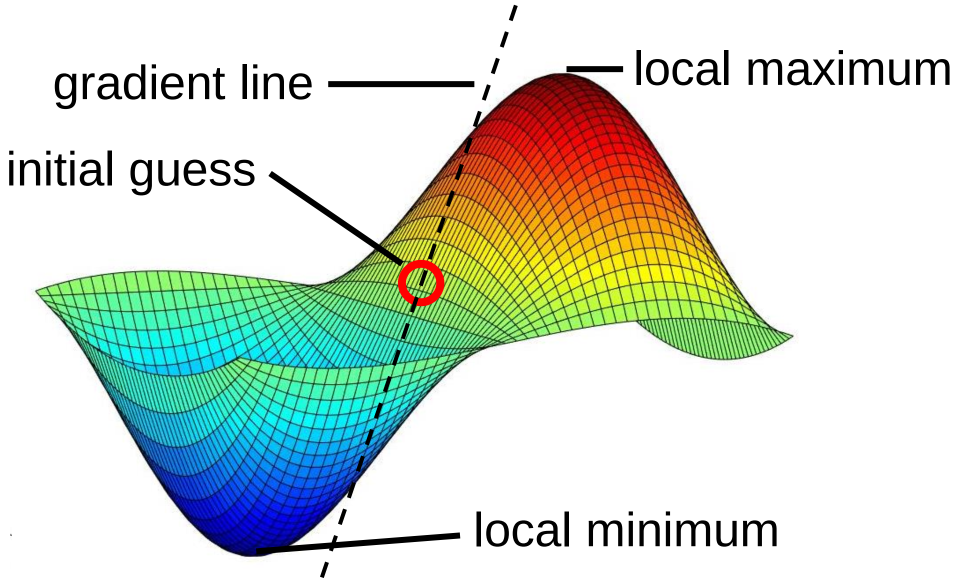

How to find the gradient?

Gradient-Based Optimization

Objective gradient can be approximated with finite difference:

1. Solve for the flow/system response and find the objective
2. Perturb a design variable by a small increment
3. Re-solve and find the new objective, approximate derivative from the difference of two states

Drawbacks: does not give exact gradients, requires solution for every design variable

Gradient-Based Optimization

Objective gradient can be obtained by solving the *tangent problem*:

$$\frac{dL}{dD_i} = \frac{\partial L}{\partial D_i} + \frac{\partial L}{\partial U_j}\left[\frac{\partial R_j}{\partial U_k}\right]^{-1}\frac{\partial R_k}{\partial D_i}$$

For every design variable D_i, solve

$$\left[\frac{\partial R_k}{\partial U_j}\right]\left\{\frac{\partial U_j}{\partial D_i}\right\} = \left\{\frac{\partial R_k}{\partial D_i}\right\}$$

Gradient-Based Optimization

Objective gradient can be obtained by solving the *tangent problem*:

Then evaluate the objective sensitivity as

$$\frac{dL}{dD_i} = \frac{\partial L}{\partial D_i} + \frac{\partial L}{\partial U_j}\frac{\partial U_j}{\partial D_i}$$

Gives exact gradients, requires solution for every design variable

Gradient-Based Optimization

Alternatively, objective gradient can be obtained using the *adjoint*:

$$\frac{dL}{dD_i} = \frac{\partial L}{\partial D_i} + \frac{\partial L}{\partial U_j}\left[\frac{\partial R_j}{\partial U_k}\right]^{-1}\frac{\partial R_k}{\partial D_i}$$

First compute the adjoint, as

$$\left[\frac{\partial R_k}{\partial U_j}\right]\{\Lambda_k\} = \left\{\frac{\partial L}{\partial U_j}\right\}$$

UNIVERSITY OF WYOMING

Gradient-Based Optimization

Alternatively, objective gradient can be obtained using the *adjoint*:

Then calculate the objective sensitivity for each design variable as

$$\frac{dL}{dD_i} = \frac{\partial L}{\partial D_i} + \Lambda_k \frac{\partial R_k}{\partial D_i}$$

Gives exact gradients, requires only one solution for all design variables

UW CFD Lab

At the University of Wyoming, the CFD lab has done years of work in general CFD applications

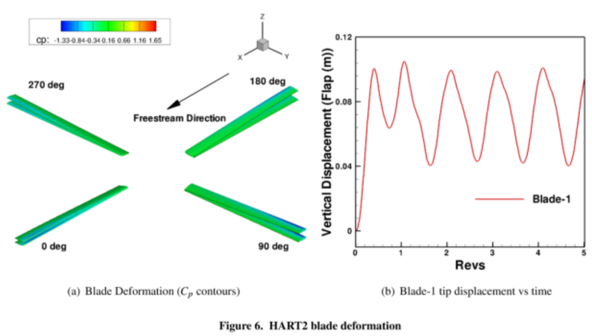

Aeroelastic response of helicopter rotor in forward flight*

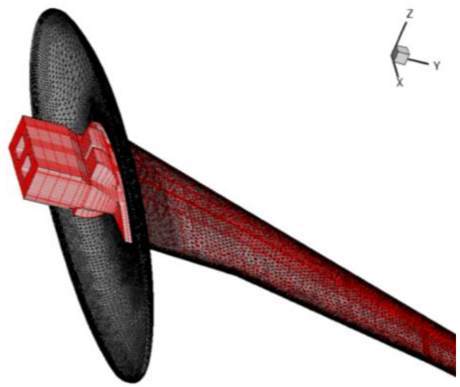

High-fidelity aero-structural model of HIRENASD wind tunnel section*

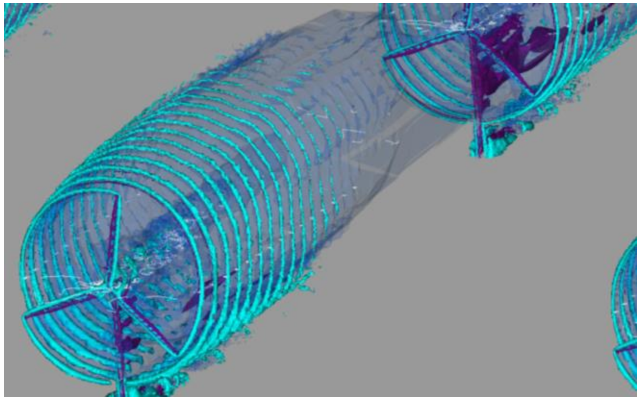

High-fidelity modeling and visualization of wind turbine wakes using high-order discontinuous Galerkin methods**

*Marviplis, D., Fabiano, E., and Anderson, E., "Recent Advances in High-Fidelity Multidisciplinary Adjoint-Based Optimization with the NSU3D Flow Solver Framework," *55th AIAA Aerospace Sciences Meeting,* CP17-1669, 2017.

**Kirby, A., Yang, Z., and Mavriplis, D., "Visualization and Data Analytics Challenges of Large-Scale High-Fidelity Numerical Simulations of Wind Energy Applications," *2018 AIAA Aerospace Sciences Meeting,* CP18-1171, 2018.

UW CFD Lab

For design and optimization of flexible aeroelastic structures, it is important to account for the coupled fluid-structural response

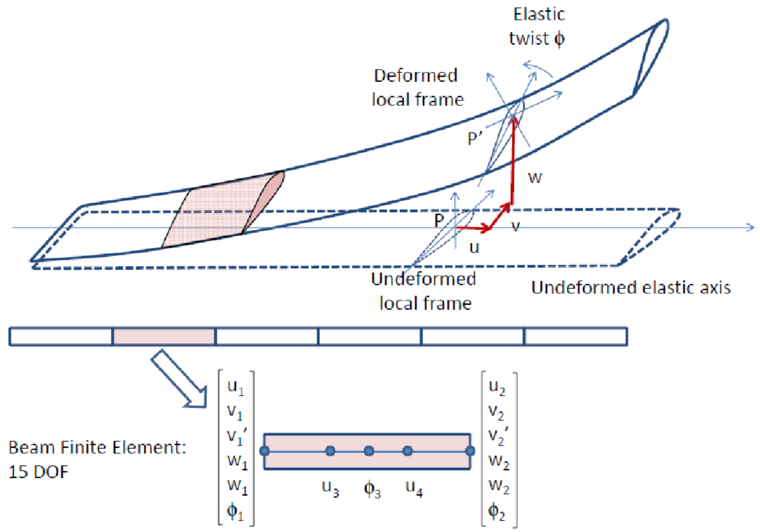

In the past many simulations have employed low-fidelity structural models. For true response and structural objectives, high fidelity structural modeling is needed.

AStrO: Adjoint-Based Structural Optimizer

AStrO has been developed as an open source FORTRAN package for high-fidelity 3D structural finite element modeling and sensitivity analysis

- Static and dynamic elastic and thermal modeling
- Linear and nonlinear geometry
- Processing input files for mesh and geometry generated by Abaqus
- Defining structural design variables (material properties, nodal coordinates, section properties)
- Obtaining exact sensitivities of user-defined objectives using the adjoint

AStrO: Fundamental Formulations

Formulation of governing equations for thermal heat conduction and elasticity:

$$\frac{\partial q_i}{\partial x_i} + \rho C_p \dot{T} - Q = 0$$

$$\frac{\partial \sigma_{ij}}{\partial x_j} - \xi \dot{u}_i - \rho \ddot{u}_i + f_i = 0$$

(PDEs)

AStrO: Fundamental Formulations

Formulation of governing equations for thermal heat conduction and elasticity:

$$\frac{\partial q_i}{\partial x_i} + \rho C_p \dot{T} - Q = 0$$

$$\frac{\partial \sigma_{ij}}{\partial x_j} - \xi \dot{u}_i - \rho \ddot{u}_i + f_i = 0$$

(PDEs)

$$\downarrow$$

$$\int_\Omega -q_i \delta\left(\frac{\partial T}{\partial x_i}\right) d\Omega + \int_\Omega \rho C_p \dot{T} \delta T d\Omega - \int_\Omega Q \delta T d\Omega + \int_S q_i n_i \delta T dS = 0$$

(Variational Form)

$$\int_\Omega \sigma_i \delta \epsilon_i d\Omega + \int_\Omega \xi \dot{u}_i \delta u_i d\Omega + \int_\Omega \rho \ddot{u}_i \delta u_i d\Omega = \int_\Omega f_i \delta u_i d\Omega + \int_S t_i \delta u_i dS$$

AStrO: Fundamental Formulations

Discretized governing equations assuming finite element solution:

$$T = N_k \phi_k$$

$$u_i = N_{ik} U_k$$

$$R_j^{\phi} = \int_{\Omega} -q_i \frac{\partial N_j}{\partial x_i} d\Omega + \int_{\Omega} \rho C_p \dot{T} N_j d\Omega - \int_{\Omega} Q N_j d\Omega + \int_{S} q_i n_i N_j dS = 0$$

$$R_j^{u} = \int_{\Omega} \sigma_i \frac{\partial \epsilon_i}{\partial U_j} d\Omega + \int_{\Omega} \xi \dot{u}_i N_{ij} d\Omega + \int_{\Omega} \rho \ddot{u}_i N_{ij} d\Omega - \int_{\Omega} f_i N_{ij} d\Omega - \int_{S} t_i N_{ij} dS = 0$$

AStrO: Fundamental Formulations

Discretized governing equations assuming finite element solution:

Thermoelastic coupling:

$$\sigma_i = C_{ik}\epsilon_k^{stress} = C_{ik}\left(\epsilon_k^{total} - \epsilon_k^{therm}\right) = C_{ik}\left(\epsilon_k^{total} - \Delta T \alpha_k^{TE}\right)$$

$$R_j^u = \int_\Omega C_{ik}\epsilon_k \frac{\partial \epsilon_i}{\partial U_j} d\Omega + \int_\Omega \xi \dot{u}_i N_{ij} d\Omega + \int_\Omega \rho \ddot{u}_i N_{ij} d\Omega - \int_\Omega f_i N_{ij} d\Omega - \int_S t_i N_{ij} dS - \int_\Omega \Delta T C_{ik} \alpha_k^{TE} \frac{\partial \epsilon_i}{\partial U_j} d\Omega = 0$$

AStrO: Fundamental Formulations

Discretized governing equations assuming finite element solution:

Implicit dynamic time integration, Newmark Beta expansion:

$$T(t+\Delta t) = T(t) + \Delta t\left((1-\gamma)\dot{T}(t) + \gamma\dot{T}(t+\Delta t)\right)$$

$$u_i(t+\Delta t) = u_i(t) + \Delta t\dot{u}_i(t) + \frac{1}{2}\Delta t^2\big((1-2\beta)\ddot{u}_i(t) + 2\beta\ddot{u}_i(t+\Delta t)\big)$$

$$\dot{u}_i(t+\Delta t) = \dot{u}_i(t) + \Delta t\big((1-\gamma)\ddot{u}_i(t) + \gamma\ddot{u}_i(t+\Delta t)\big)$$

$$0 < \gamma \leq 1$$

$$0 < \beta \leq \frac{1}{2}$$

AStrO: Fundamental Formulations

Element library supports solid continuum, shell, and beam elements

Solid Elements:

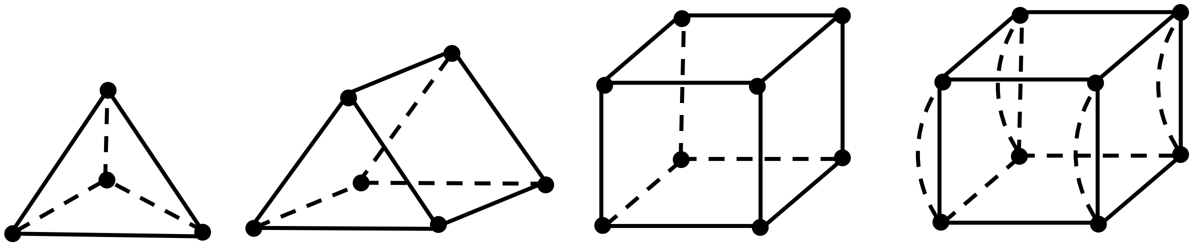

(Incompatible modes)

Shell Elements:

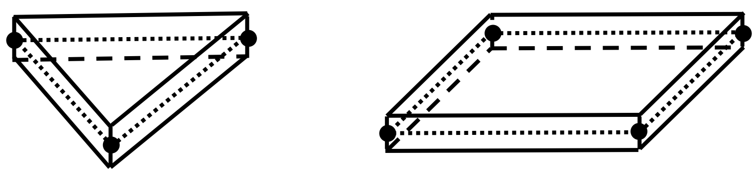

Beam Elements:

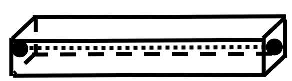

AStrO: Fundamental Formulations

Solid continuum elements:

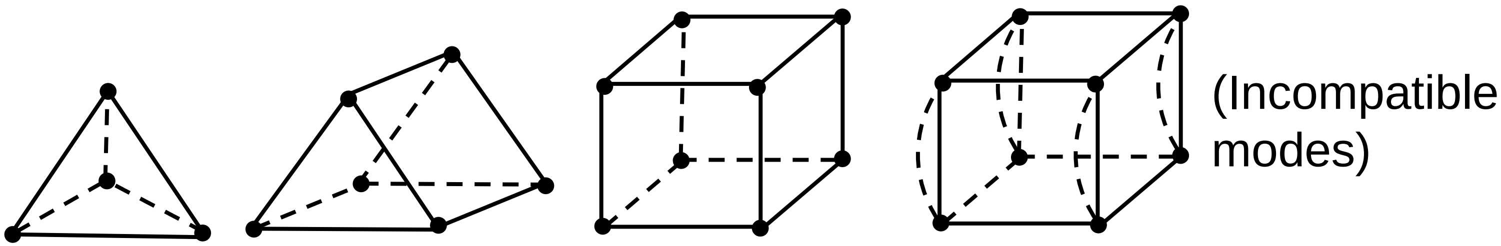

Elastic solution completely defined by nodal displacements:

$$u_i = N_{ik} U_k$$

Green-Lagrange strain definition:

$$\epsilon_{ip} = \frac{1}{2}\left(\frac{\partial u_i}{\partial x_p} + \frac{\partial u_p}{\partial x_i} + \underbrace{\frac{\partial u_q}{\partial x_i}\frac{\partial u_q}{\partial x_p}}_{\text{Nonlinear term}}\right)$$

AStrO: Fundamental Formulations

Shell elements, derived from Kirchhoff plate theory:

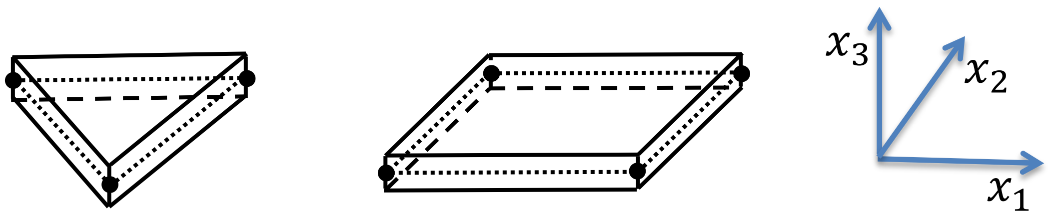

Nodal displacements ***and*** rotations defined at midplane:

$$u_i^m = U_{ij} N_j$$
$$\theta_i = \theta_{ij} N_j$$

3D displacement field:

$$u_1 = u_1^m + x_3 \theta_2$$
$$u_2 = u_2^m - x_3 \theta_1$$
$$u_3 = u_3^m$$

Strain definition:

$$\epsilon_{ip} = \frac{1}{2}\left(\frac{\partial u_i}{\partial x_p} + \frac{\partial u_p}{\partial x_i}\right)$$

(Coordinate transformation for nonlinear geometry)

UNIVERSITY OF WYOMING

AStrO: Fundamental Formulations

Beam elements, Bernoulli beam theory:

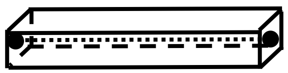

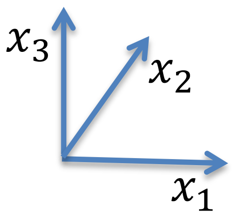

Nodal displacements ***and*** rotations defined at midplane:

$$u_i^m = U_{ij} N_j$$
$$\theta_i = \theta_{ij} N_j$$

3D displacement field:

$$u_1 = u_1^m + x_3 \theta_2 - x_2 \theta_3$$
$$u_2 = u_2^m$$
$$u_3 = u_3^m$$

(Principle of virtual work formulated in terms of normal strain, curvature twist using A, E, I, G, J)

AStrO: Adjoint-Based Sensitivities

Recall the general procedure for adjoint-based sensitivities:

$$(1)\ solve \quad \left[\frac{\partial \boldsymbol{R}}{\partial \boldsymbol{U}}\right]^T \{\boldsymbol{\Lambda}\} = \left\{\frac{\partial L}{\partial \boldsymbol{U}}\right\}$$

$$(2)\ for\ every\ design\ variable, compute$$

$$\frac{dL}{dD_i} = \frac{\partial L}{\partial D_i} + \lfloor \boldsymbol{\Lambda}^T \rfloor \left\{\frac{\partial \boldsymbol{R}}{\partial D_i}\right\}$$

AStrO: Adjoint-Based Sensitivities

Recall the general procedure for adjoint-based sensitivities:

$$(1)\ solve\ \left[\frac{\partial \boldsymbol{R}}{\partial \boldsymbol{U}}\right]^T \{\boldsymbol{\Lambda}\} = \left\{\frac{\partial L}{\partial \boldsymbol{U}}\right\}$$

Critical components for any discipline

$$(2)\ for\ every\ design\ variable, compute$$

$$\frac{dL}{dD_i} = \frac{\partial L}{\partial D_i} + \lfloor \boldsymbol{\Lambda}^T \rfloor \left\{\frac{\partial \boldsymbol{R}}{\partial D_i}\right\}$$

AStrO: Adjoint-Based Sensitivities

Categories of design variables supported by AStrO:

1) Elastic properties (Young's modulus, Poisson's ratio, etc.)
2) Mass density
3) Thermal conductivity
4) Coefficient of thermal expansion
5) Specific heat capacity
6) Local material orientation
7) Cross-sectional properties (for shells and beams only)
8) Nodal coordinates
9) Applied mechanical load (body force and tractions)
10) Applied thermal load (internal heat generation and surface flux)

(May be defined in separate input file)

AStrO: Adjoint-Based Sensitivities

Summary of thermoelastic governing equations:

$$\mathit{Heat\ Conduction, Poisson\ Equation}:$$

$$R_j^{\phi,n+1} = R_j^{\phi,k,n+1} + R_j^{\phi,m,n+1} + R_j^{\phi,hg,n+1} = 0$$

$$R_j^{\dot{\phi},n+1} = \phi_j^{n+1} - \phi_j^n - \Delta t\left((1-\gamma)\dot{\phi}_j^n + \gamma\dot{\phi}_j^{n+1}\right) = 0$$

$$0 < \gamma \le 1$$

$$R_j^{\phi,k} = \int_\Omega -q_i \frac{\partial N_j}{\partial x_i} d\Omega = K_{jq}^{\phi}\phi_q$$

$$R_j^{\phi,m} = \int_\Omega \rho C_p N_q \dot{\phi}_q N_j d\Omega = M_{jq}^{\phi}\dot{\phi}_q$$

$$R_j^{\phi,hg} = -\int_\Omega Q N_j d\Omega + \int_S q_i n_i N_j dS$$

$$\mathit{Elasticity, Principle\ of\ Virtual\ Work}:$$

$$R_j^{u,n+1} = (1+\alpha)\left(R_j^{u,k,n+1} + R_j^{u,c,n+1} - R_j^{u,app,n+1} - R_j^{u,th,n+1}\right) \\ -\alpha\left(R_j^{u,k,n} + R_j^{u,c,n} - R_j^{u,app,n} - R_j^{u,th,n}\right) + R_j^{u,m,n+1} = 0$$

$$R_j^{\ddot{u},n+1} = U_j^{n+1} - U_j^n - \Delta t\dot{U}_j^n - \frac{1}{2}\Delta t^2\left((1-2\beta)\ddot{U}_j^n + 2\beta\ddot{U}_j^{n+1}\right) = 0$$

$$R_j^{\dot{u},n+1} = \dot{U}_j^{n+1} - \dot{U}_j^n - \Delta t\left((1-\gamma)\ddot{U}_j^n + \gamma\ddot{U}_j^{n+1}\right) = 0$$

$$0 < \beta \le \frac{1}{2}$$
$$0 < \gamma \le 1$$
$$-1 < \alpha \le 0$$

$$R_j^{u,k} = \int_\Omega C_{ik}\epsilon_k \frac{\partial \epsilon_i}{\partial U_j} d\Omega$$

$$R_j^{u,c} = \int_\Omega \xi N_{iq}\dot{U}_q N_{ij} d\Omega = C_{jq}^u \dot{U}_q$$

$$R_j^{u,m} = \int_\Omega \rho N_{iq}\ddot{U}_q N_{ij} d\Omega = M_{jq}^u \ddot{U}_q$$

$$R_j^{u,app} = -\int_\Omega f_i N_{ij} d\Omega - \int_S t_i N_{ij} dS$$

$$R_j^{u,th} = \int_\Omega N_q \phi_q C_{ik}\alpha_k^{TE} \frac{\partial \epsilon_i}{\partial U_j} d\Omega$$

AStrO: Adjoint-Based Sensitivities

For static analysis:

$$\left[\frac{\partial \boldsymbol{R}}{\partial \boldsymbol{U}}\right] = \begin{bmatrix} \left[\frac{\partial \boldsymbol{R}^{\phi}}{\partial \boldsymbol{\phi}}\right] & 0 \\ \left[\frac{\partial \boldsymbol{R}^{u}}{\partial \boldsymbol{\phi}}\right] & \left[\frac{\partial \boldsymbol{R}^{u}}{\partial \boldsymbol{U}}\right] \end{bmatrix}$$

(Adjoint has components for both displacement $\boldsymbol{U}$ and temperature $\boldsymbol{\phi}$. Either discipline can be omitted for single-disciplinary analysis.)

AStrO: Adjoint-Based Sensitivities

For dynamic analysis:

$$\boldsymbol{U} = \begin{Bmatrix} \boldsymbol{U}^0 \\ \boldsymbol{U}^1 \\ \boldsymbol{U}^2 \\ \boldsymbol{U}^3 \\ \vdots \end{Bmatrix} \quad \boldsymbol{R} = \begin{Bmatrix} \boldsymbol{R}^0(\boldsymbol{U}^0) \\ \boldsymbol{R}^1(\boldsymbol{U}^0, \boldsymbol{U}^1) \\ \boldsymbol{R}^2(\boldsymbol{U}^1, \boldsymbol{U}^2) \\ \boldsymbol{R}^3(\boldsymbol{U}^2, \boldsymbol{U}^3) \\ \vdots \end{Bmatrix}$$

$$\left[\frac{\partial \boldsymbol{R}}{\partial \boldsymbol{U}}\right] = \begin{bmatrix} \left[\frac{\partial \boldsymbol{R}^0}{\partial \boldsymbol{U}^0}\right] & 0 & 0 & 0 & \cdots \\ \left[\frac{\partial \boldsymbol{R}^1}{\partial \boldsymbol{U}^0}\right] & \left[\frac{\partial \boldsymbol{R}^1}{\partial \boldsymbol{U}^1}\right] & 0 & 0 & \cdots \\ 0 & \left[\frac{\partial \boldsymbol{R}^2}{\partial \boldsymbol{U}^1}\right] & \left[\frac{\partial \boldsymbol{R}^2}{\partial \boldsymbol{U}^2}\right] & 0 & \cdots \\ 0 & 0 & \left[\frac{\partial \boldsymbol{R}^3}{\partial \boldsymbol{U}^2}\right] & \left[\frac{\partial \boldsymbol{R}^3}{\partial \boldsymbol{U}^3}\right] & \cdots \\ \vdots & \vdots & \vdots & \ddots & \ddots \end{bmatrix}$$

AStrO: Adjoint-Based Sensitivities

For dynamic analysis:

$$
\begin{bmatrix}
\ddots & \ddots & \vdots & \vdots & \vdots \\
\cdots & \left[\frac{\partial \boldsymbol{R}^{m-3}}{\partial \boldsymbol{U}^{m-3}}\right]^T & \left[\frac{\partial \boldsymbol{R}^{m-2}}{\partial \boldsymbol{U}^{m-3}}\right]^T & 0 & 0 \\
\cdots & 0 & \left[\frac{\partial \boldsymbol{R}^{m-2}}{\partial \boldsymbol{U}^{m-2}}\right]^T & \left[\frac{\partial \boldsymbol{R}^{m-1}}{\partial \boldsymbol{U}^{m-2}}\right]^T & 0 \\
\cdots & 0 & 0 & \left[\frac{\partial \boldsymbol{R}^{m-1}}{\partial \boldsymbol{U}^{m-1}}\right]^T & \left[\frac{\partial \boldsymbol{R}^{m}}{\partial \boldsymbol{U}^{m-1}}\right]^T \\
\cdots & 0 & 0 & 0 & \left[\frac{\partial \boldsymbol{R}^{m}}{\partial \boldsymbol{U}^{m}}\right]^T
\end{bmatrix}
\begin{Bmatrix}
\vdots \\ \boldsymbol{\Lambda}^{m-3} \\ \boldsymbol{\Lambda}^{m-2} \\ \boldsymbol{\Lambda}^{m-1} \\ \boldsymbol{\Lambda}^{m}
\end{Bmatrix}
=
\begin{Bmatrix}
\vdots \\ \frac{\partial L}{\partial \boldsymbol{U}^{m-3}} \\ \frac{\partial L}{\partial \boldsymbol{U}^{m-2}} \\ \frac{\partial L}{\partial \boldsymbol{U}^{m-1}} \\ \frac{\partial L}{\partial \boldsymbol{U}^{m}}
\end{Bmatrix}
$$

AStrO: Adjoint-Based Sensitivities

$$
\left[\frac{\partial \boldsymbol{R}^{n+1}}{\partial \boldsymbol{U}^{n}}\right] = \begin{bmatrix}
\left[\frac{\partial \boldsymbol{R}^{\phi,n+1}}{\partial \boldsymbol{\phi}^{n}}\right] & \left[\frac{\partial \boldsymbol{R}^{\phi,n+1}}{\partial \dot{\boldsymbol{\phi}}^{n}}\right] & 0 & 0 & 0 \\
\left[\frac{\partial \boldsymbol{R}^{\dot{\phi},n+1}}{\partial \boldsymbol{\phi}^{n}}\right] & \left[\frac{\partial \boldsymbol{R}^{\dot{\phi},n+1}}{\partial \dot{\boldsymbol{\phi}}^{n}}\right] & 0 & 0 & 0 \\
\left[\frac{\partial \boldsymbol{R}^{u,n+1}}{\partial \boldsymbol{\phi}^{n}}\right] & 0 & \left[\frac{\partial \boldsymbol{R}^{u,n+1}}{\partial \boldsymbol{U}^{n}}\right] & \left[\frac{\partial \boldsymbol{R}^{u,n+1}}{\partial \ddot{\boldsymbol{U}}^{n}}\right] & \left[\frac{\partial \boldsymbol{R}^{u,n+1}}{\partial \dot{\boldsymbol{U}}^{n}}\right] \\
0 & 0 & \left[\frac{\partial \boldsymbol{R}^{\ddot{u},n+1}}{\partial \boldsymbol{U}^{n}}\right] & \left[\frac{\partial \boldsymbol{R}^{\ddot{u},n+1}}{\partial \ddot{\boldsymbol{U}}^{n}}\right] & \left[\frac{\partial \boldsymbol{R}^{\ddot{u},n+1}}{\partial \dot{\boldsymbol{U}}^{n}}\right] \\
0 & 0 & 0 & \left[\frac{\partial \boldsymbol{R}^{\dot{u},n+1}}{\partial \ddot{\boldsymbol{U}}^{n}}\right] & \left[\frac{\partial \boldsymbol{R}^{\dot{u},n+1}}{\partial \dot{\boldsymbol{U}}^{n}}\right]
\end{bmatrix}
$$

(Diagonal block lower-triangular for solution, upper triangular for adjoint.)

$$
\left[\frac{\partial \boldsymbol{R}^{n+1}}{\partial \boldsymbol{U}^{n+1}}\right] = \begin{bmatrix}
\left[\frac{\partial \boldsymbol{R}^{\phi,n+1}}{\partial \boldsymbol{\phi}^{n+1}}\right] & 0 & 0 & 0 & 0 \\
\left[\frac{\partial \boldsymbol{R}^{\dot{\phi},n+1}}{\partial \boldsymbol{\phi}^{n+1}}\right] & \left[\frac{\partial \boldsymbol{R}^{\dot{\phi},n+1}}{\partial \dot{\boldsymbol{\phi}}^{n+1}}\right] & 0 & 0 & 0 \\
\left[\frac{\partial \boldsymbol{R}^{u,n+1}}{\partial \boldsymbol{\phi}^{n+1}}\right] & 0 & \left[\frac{\partial \boldsymbol{R}^{u,n+1}}{\partial \boldsymbol{U}^{n+1}}\right] & 0 & 0 \\
0 & 0 & \left[\frac{\partial \boldsymbol{R}^{\ddot{u},n+1}}{\partial \boldsymbol{U}^{n+1}}\right] & \left[\frac{\partial \boldsymbol{R}^{\ddot{u},n+1}}{\partial \ddot{\boldsymbol{U}}^{n+1}}\right] & 0 \\
0 & 0 & 0 & \left[\frac{\partial \boldsymbol{R}^{\dot{u},n+1}}{\partial \ddot{\boldsymbol{U}}^{n+1}}\right] & \left[\frac{\partial \boldsymbol{R}^{\dot{u},n+1}}{\partial \dot{\boldsymbol{U}}^{n+1}}\right]
\end{bmatrix}
$$

AStrO: Adjoint-Based Sensitivities

Sensitivities of governing equations obtained through linearization of the original analysis code:

Term	$\frac{\partial}{\partial D}$
$R_j^{\phi,k}$	$-\int_\eta \left(\frac{\partial q_i}{\partial D} \frac{\partial N_j}{\partial x_i} J^{Det} + q_i \frac{\partial}{\partial D}\left(\frac{\partial N_j}{\partial x_i}\right) J^{Det} + q_i \frac{\partial N_j}{\partial x_i} \frac{\partial J^{Det}}{\partial D} \right) d\eta$
$R_j^{\phi,m}$	$\int_\eta \left(\frac{\partial \rho}{\partial D} C_p J^{Det} + \rho \frac{\partial C_p}{\partial D} J^{Det} + \rho C_p \frac{\partial J^{Det}}{\partial D} \right) N_q \dot{\phi}_q N_j d\eta$
$R_j^{u,k}$	$\int_\eta \left(\frac{\partial C_{ik}}{\partial D} \epsilon_k \frac{\partial \epsilon_i}{\partial U_j} J^{Det} + C_{ik} \frac{\partial \epsilon_k}{\partial D} \frac{\partial \epsilon_i}{\partial U_j} J^{Det} + C_{ik}\epsilon_k \frac{\partial}{\partial D}\left(\frac{\partial \epsilon_i}{\partial U_j}\right) J^{Det} + C_{ik}\epsilon_k \frac{\partial \epsilon_i}{\partial U_j} \frac{\partial J^{Det}}{\partial D} \right) d\eta$
$R_j^{u,c}$	$\int_\eta \left(\frac{\partial \xi}{\partial D} J^{Det} + \xi \frac{\partial J^{Det}}{\partial D} \right) N_{iq} \dot{U}_q N_{ij} d\eta$
$R_j^{u,m}$	$\int_\eta \left(\frac{\partial \rho}{\partial D} J^{Det} + \rho \frac{\partial J^{Det}}{\partial D} \right) N_{iq} \ddot{U}_q N_{ij} d\eta$
$R_j^{u,th}$	$\int_\eta \left(\frac{\partial C_{ik}}{\partial D} \alpha_k^{TE} \frac{\partial \epsilon_i}{\partial U_j} J^{Det} + C_{ik} \frac{\partial \alpha_k^{TE}}{\partial D} \frac{\partial \epsilon_i}{\partial U_j} J^{Det} + C_{ik}\alpha_k^{TE} \frac{\partial}{\partial D}\left(\frac{\partial \epsilon_i}{\partial U_j}\right) J^{Det} + C_{ik}\alpha_k^{TE} \frac{\partial \epsilon_i}{\partial U_j} \frac{\partial J^{Det}}{\partial D} \right) N_q \phi_q d\eta$

Fluid-Structure Interface

AStrO couples with NSU3D CFD code through fluid-structure interface

- **Outer loop over physical time steps**
  - **Coupling iterations per time step :**
    - Fluid Mesh:
      - Line implicit multigrid
    - Flow:
      - Implicit BDF2 Newton iterations (GMRES)
      - Linear agglomeration multi-grid
    - FSI (Fluid to structure)
      - Explicit assignment

$$\{F\}_{CSD} = [T]\{F\}_{CFD}$$

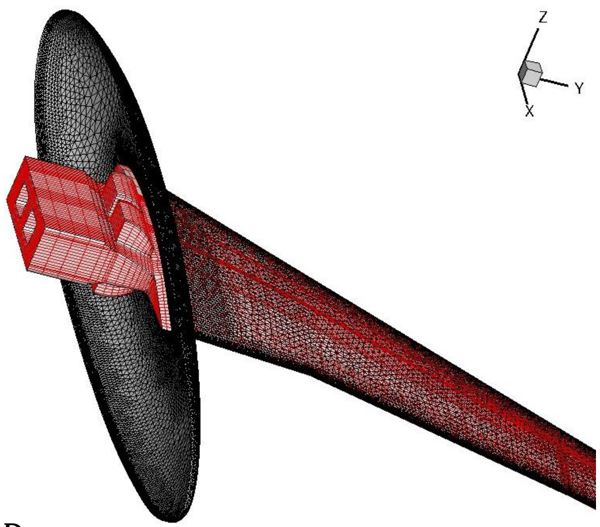

    - Structure:
      - Solve via designated method (direct, iterative, MUMPS, etc.)
    - FSI (Structure to fluid)
      - Explicit assignment

$$\{U\}_{CFD} = [T]^T\{U\}_{CSD}$$

Fluid-Structure Interface

FSI coupling iteration process continues until the solution converges

Initial deflection (1st coupling) = 4.5m

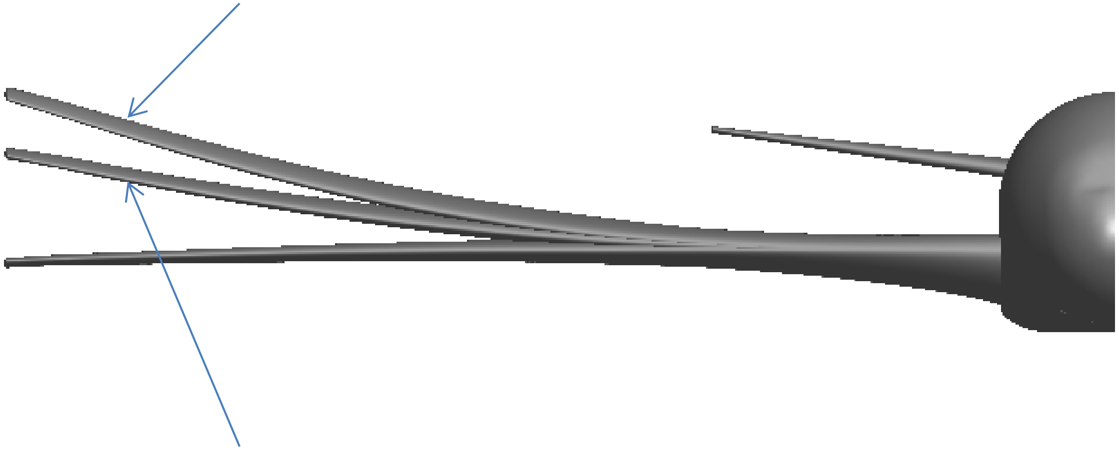

Final deflection (last coupling) = 2.9m

Demonstrations and Validations

Static thermoelastic response of solid cube:

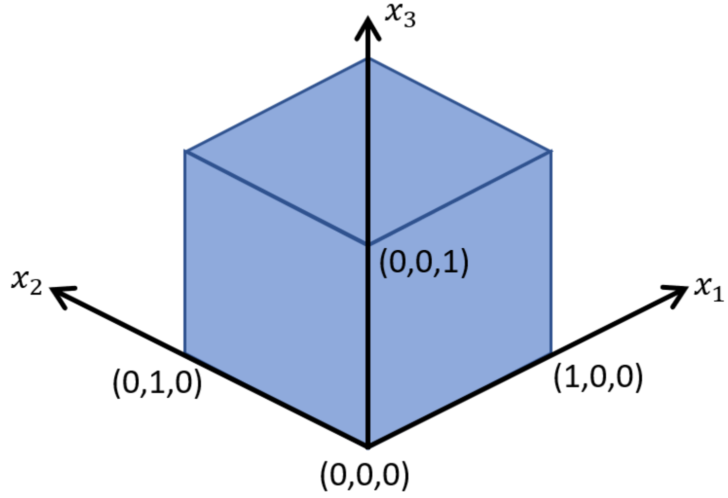

C_{ij} = Elastic stiffness matrix

α^{TE}= Coefficient of thermal expansion

k= Thermal conductivity

Internal heat generation: $$Q = \frac{\partial q_i}{\partial x_i} = -\frac{2k}{\alpha^{TE}}\left(\frac{C_{11}}{(C_{11}+C_{12}+C_{13})} + \frac{C_{22}}{(C_{21}+C_{22}+C_{23})} + \frac{C_{33}}{(C_{31}+C_{32}+C_{33})}\right)10^{-3}$$

Surface flux: $$q_i = -k\frac{\partial T}{\partial x_i} = -\frac{2k}{\alpha^{TE}}\left[\frac{(C_{11}x_1+C_{44}+C_{55})}{(C_{11}+C_{12}+C_{13})}, \frac{(C_{22}x_2+C_{44}+C_{66})}{(C_{21}+C_{22}+C_{23})}, \frac{(C_{33}x_3+C_{55}+C_{66})}{(C_{31}+C_{32}+C_{33})}\right]10^{-3}$$

Demonstrations and Validations

Static thermoelastic response of solid cube:

Temperature solution:

$$T = \frac{2}{\alpha^{TE}}\left(\frac{\left(\frac{1}{2}C_{11}x_1 + C_{44} + C_{55}\right)x_1}{(C_{11} + C_{12} + C_{13})} + \frac{\left(\frac{1}{2}C_{22}x_2 + C_{44} + C_{66}\right)x_2}{(C_{21} + C_{22} + C_{23})} + \frac{\left(\frac{1}{2}C_{33}x_3 + C_{55} + C_{66}\right)x_3}{(C_{31} + C_{32} + C_{33})}\right)10^{-3}$$

Displacement solution:

$$u_1 = \left(\frac{1}{3}x_1^3 + x_2^2 + x_3^2\right)10^{-3}$$

$$u_2 = \left(x_1^2 + \frac{1}{3}x_2^3 + x_3^2\right)10^{-3}$$

$$u_3 = \left(x_1^2 + x_2^2 + \frac{1}{3}x_3^3\right)10^{-3}$$

Strain solution:

$$\epsilon_1 = \frac{\partial u_1}{\partial x_1} = x_1^2 10^{-3} \qquad \gamma_{12} = \frac{\partial u_1}{\partial x_2} + \frac{\partial u_2}{\partial x_1} = 2(x_1 + x_2)10^{-3}$$

$$\epsilon_2 = \frac{\partial u_2}{\partial x_2} = x_2^2 10^{-3} \qquad \gamma_{13} = \frac{\partial u_1}{\partial x_3} + \frac{\partial u_3}{\partial x_1} = 2(x_1 + x_3)10^{-3}$$

$$\epsilon_3 = \frac{\partial u_3}{\partial x_3} = x_3^2 10^{-3} \qquad \gamma_{23} = \frac{\partial u_2}{\partial x_3} + \frac{\partial u_3}{\partial x_2} = 2(x_2 + x_3)10^{-3}$$

Demonstrations and Validations

Temperature and displacement response for (a) eight-node hexahedral elements (b) four-node tetrahedral elements:

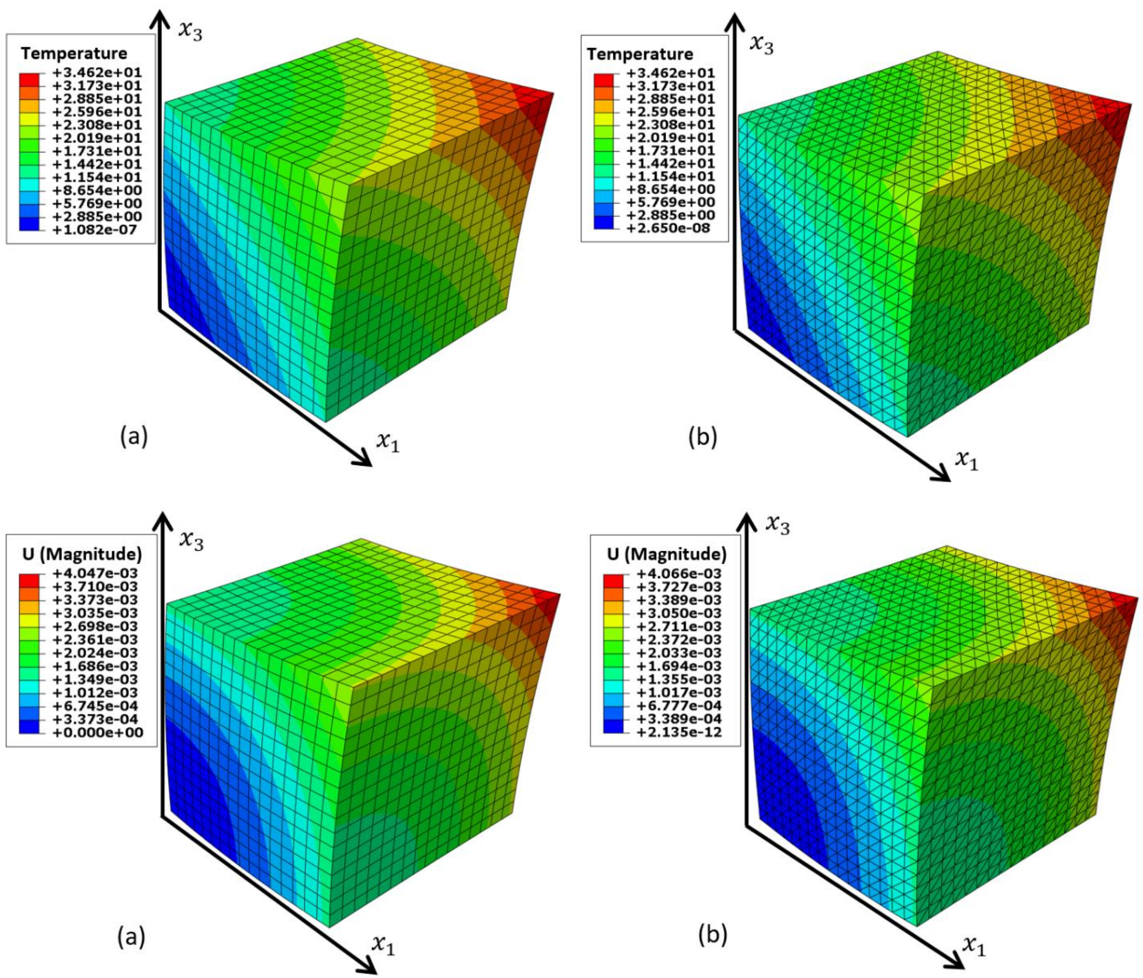

Demonstrations and Validations

Mesh convergence of thermoelastic solution of solid cube:

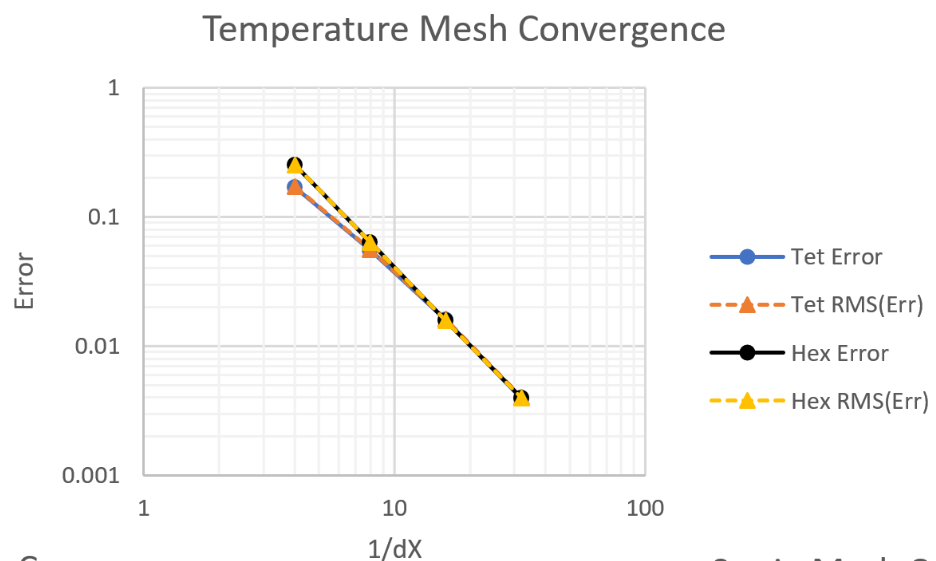

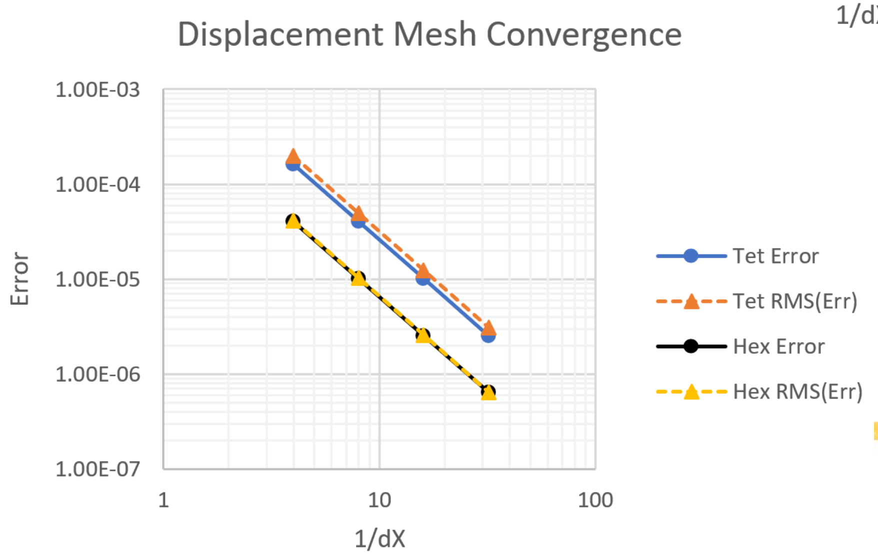

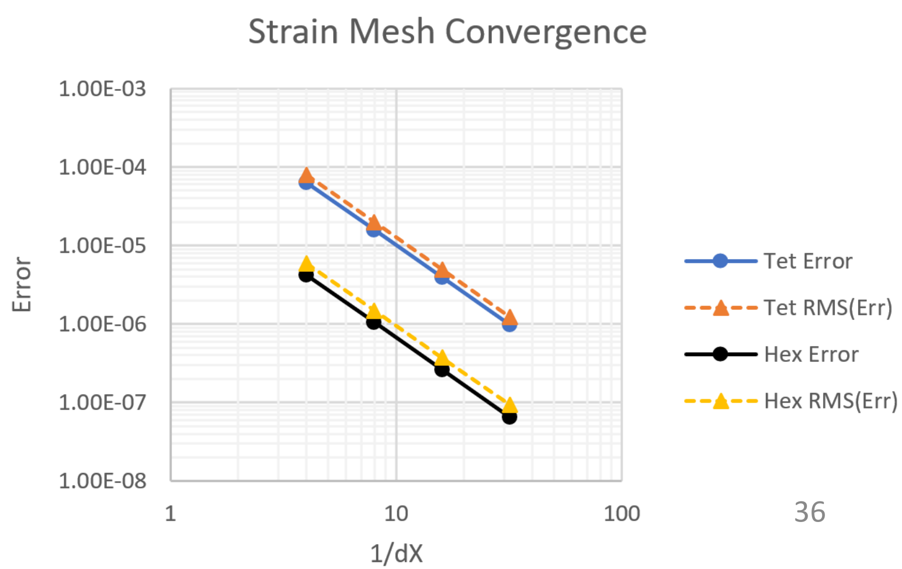

Demonstrations and Validations

Sensitivities of normal strain at center of cube:

Hex elements:

	Adjoint	**Tangent**	**Complex**
E	1.016231638217**54**E+02	1.016231638217**40**E+02	1.016231638217**49**E+02
k	-3.19733746691863E+01	-3.19733746691863E+01	-3.19733746691863E+01
α^{TE}	4.591523458546**06**E+01	4.591523458546**10**E+01	4.591523458546**07**E+01

Hex elements with incompatible modes:

	Adjoint	**Tangent**	**Complex**
E	1.020040590717**04**E+02	1.020040590717**15**E+02	1.020040590717**40**E+02
k	-3.23030013695860E+01	-3.23030013695860E+01	-3.23030013695860E+01
α^{TE}	4.396485644427**60**E+01	4.396485644427**94**E+01	4.396485644427**69**E+01

Tet elements:

	Adjoint	**Tangent**	**Complex**
E	4.421185706005**18**E+02	4.421185706005**08**E+02	4.421185706005**73**E+02
k	-4.0243937862772**8**E+01	-4.0243937862772**7**E+01	-4.024393786277**40**E+01
α^{TE}	2.6201358577098**4**E+02	2.6201358577098**7**E+02	2.6201358577098**8**E+02

Demonstrations and Validations

NACA 0012 section in free vibration:

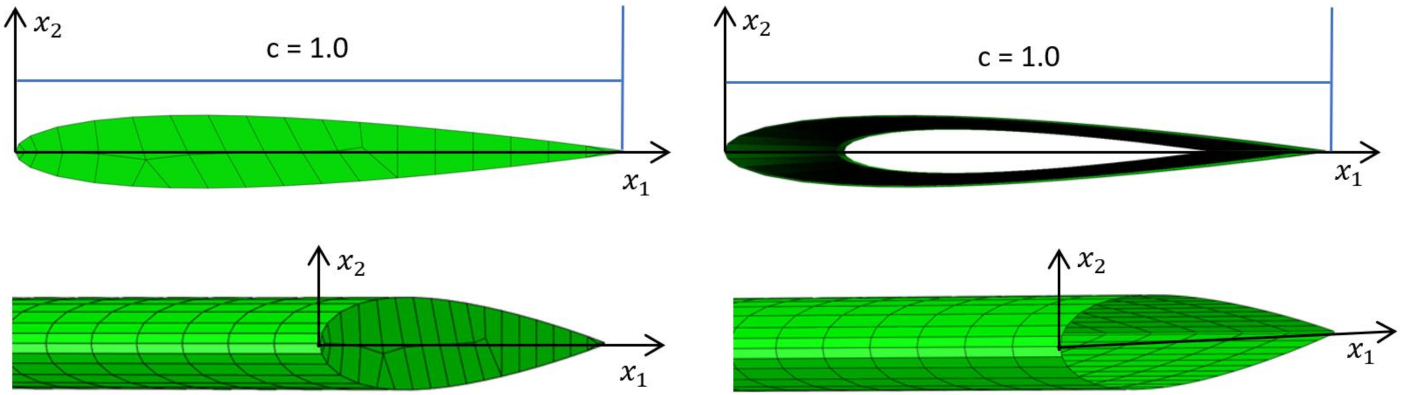

$$u_2 = \left(\cosh(\beta x_3) - \cos(\beta x_3) - \alpha(\sinh(\beta x_3) - \sin(\beta x_3))\right)(1 - \cos(\omega t))$$

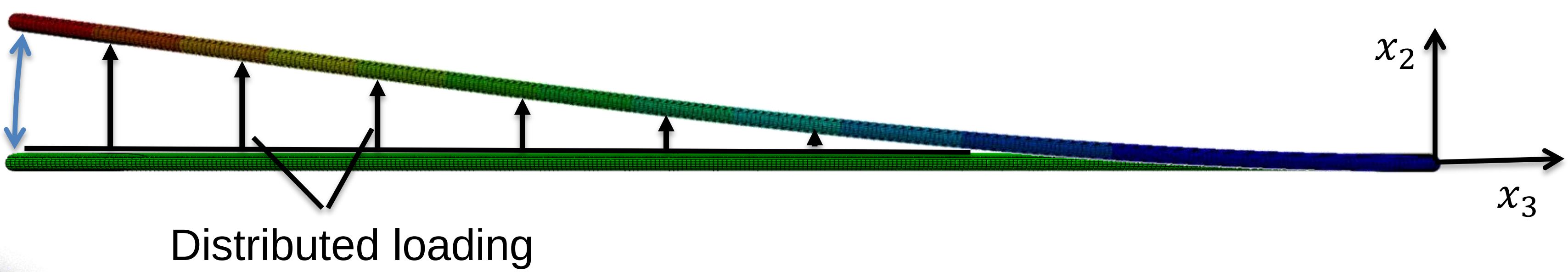

Demonstrations and Validations

NACA 0012 section in free vibration:

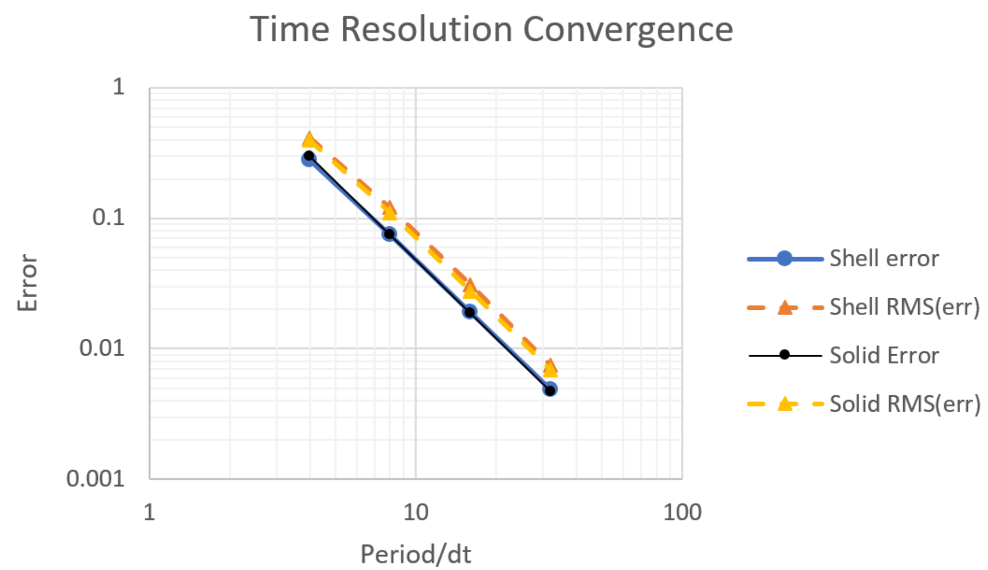

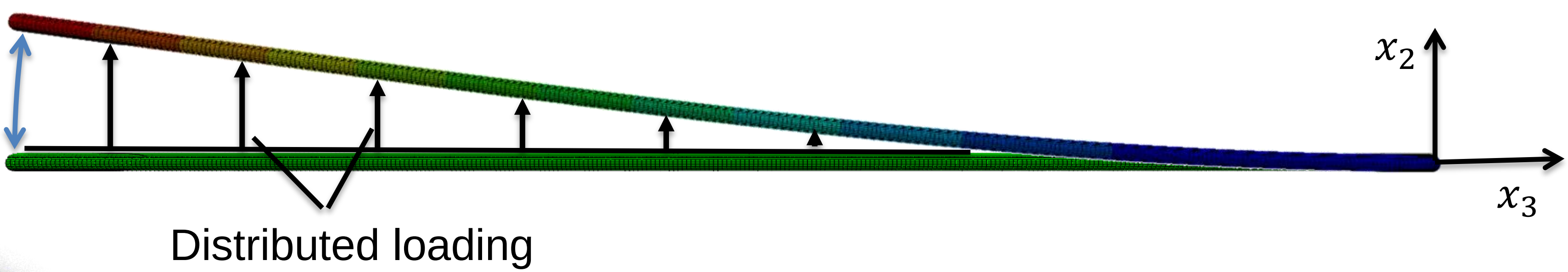

Demonstrations and Validations

Sensitivities of cumulative tip deflection of NACA 0012 section:

Shell model:

	Adjoint	Tangent	Complex
Modulus	-2.28662547511174E+01	-2.28662547511176E+01	-2.28662547511172E+01
Density	6.80909337379652E+00	6.80909337379656E+00	6.80909337379659E+00
Thickness	-6.87938499499907E-02	-6.87938499499919E-02	-6.87938499499910E-02
X3	7.11201895842075E+01	7.11201895843516E+01	7.11201895847536E+01

Solid model:

	Adjoint	Tangent	Complex
Modulus	-2.34316797685626E+01	-2.34316797685609E+01	-2.34316797685665E+01
Density	6.93622330325826E+00	6.93622330325728E+00	6.93622330325849E+00
X3	7.69163259198577E+01	7.69163259198956E+01	7.69163259198118E+01

Demonstrations and Validations

Demonstration: 1st mode free vibration test of HIRENASD* wing, clamped at root. Response computed with Newmark Beta-HHT alpha implicit time integration.

First mode vibration displacement contour on deformed HIRENASD wing

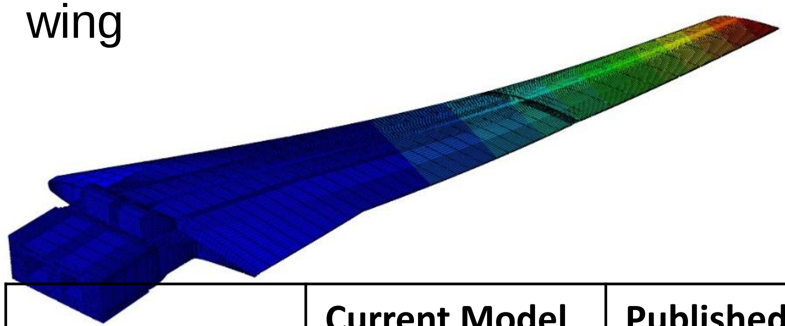

	Current Model	Published
Natural Frequency	26.55 Hz	26.53 Hz

Tip displacement history of HIRENASD wing in free vibration

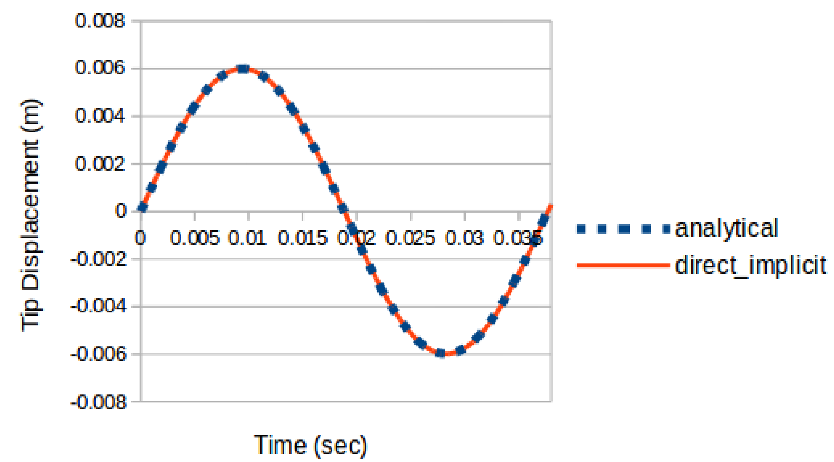

*Reimer, L., Boucke, A., Ballmann, J., and Behr, M. "Computational Analysis of High-Reynolds Number Aero-Structural Dynamics HIRENASD," *International Forum of Aeroelasticity and Structural Dynamics* CP2009-130, 2009

Demonstrations and Validations

Demonstration: Coupled aero-structural simulation of HIRENASD wing model computed lift coefficient of 0.3304 compares well with published value

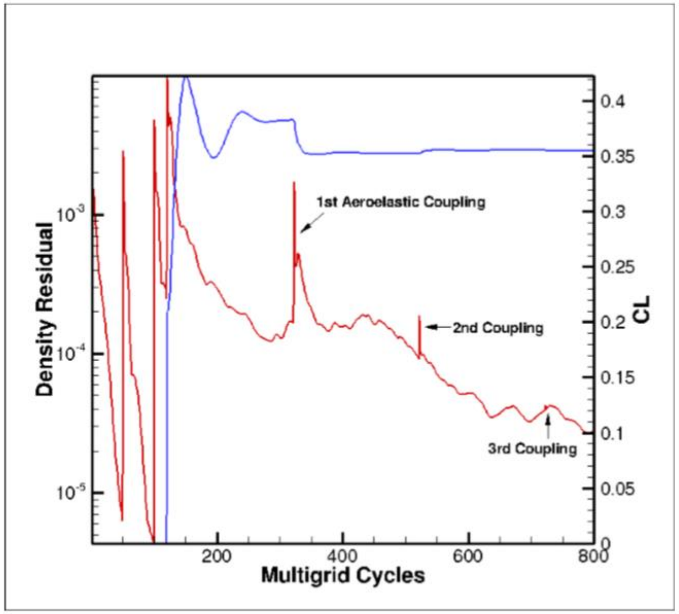

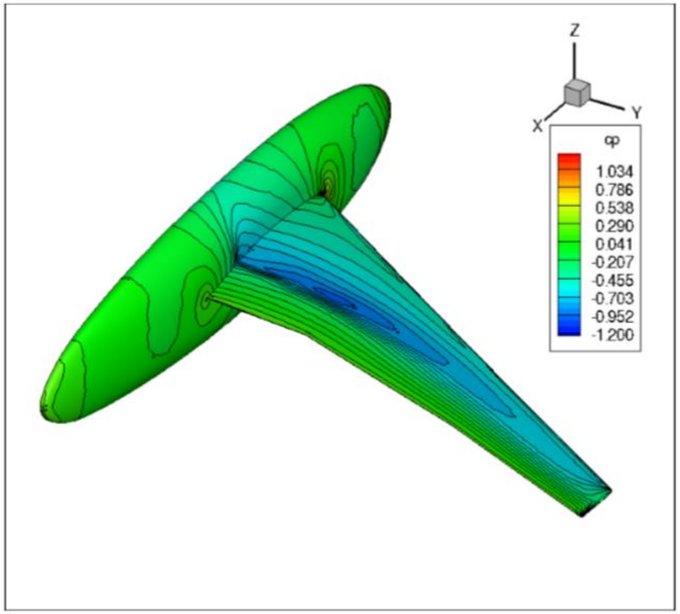

Case Study: Fatigue Stress Minimization on SWiFT Wind Turbine Blade

- Longevity of wind turbines is critical for economic viability.
- Fatigue damage is a major contributor to failure in turbines.
- Extension of work by Bhuiyan *et al.** was performed to minimize fatigue-driving stress under simulated loading.

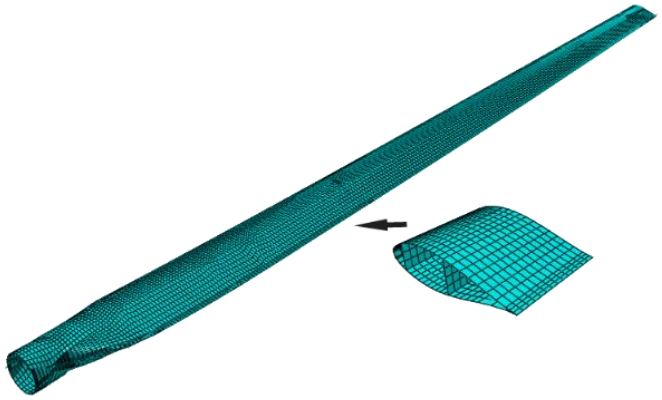

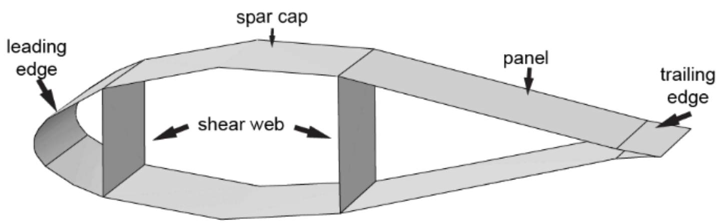

SWiFT wind blade model**

*Bhuiyan, Faisal Hasan, Mavriplis, Dimitri and Fertig, Ray S., "Predicting Composite Fatigue Life of Wind Turbine Blades Using Constituent-Level Physics and Realistic Aerodynamic Load," *57th AIAA/ASCE/AHS/ASC Structures, Structural Dynamics, and Materials Conference*, CP988, 2016.

**Resor, B. R. and LeBlanc, B., "An Aeroelastic Reference Model for the SWiFT Turbines," Sandia National Laboratories, Rept. SAND2014-19136, Albuquerque, NM, Oct. 2014.

Case Study: Fatigue Stress Minimization on SWiFT Wind Turbine Blade

Fatigue damage in polymers has been shown to be well-modeled using the kinetic theory of fracture:

$$\frac{dn}{dt} = (n_0 - n)^{\lambda} \frac{kT}{h} \exp\left(\frac{\gamma \sigma^{eff} - U}{kT}\right)$$

n = damage parameter between 0 and 1.
λ, γ, U = material dependent constants.
h = Planck's constant
k = Boltzmann's constant
T = Absolute temperature

In fiber-reinforced composites, the challenge lies in the identification of the effective scalar stress criterion σ^{eff}.

Case Study: Fatigue Stress Minimization on SWiFT Wind Turbine Blade

Effective off-axis matrix stress in fiber-reinforced composites developed by Fertig *et al.**:

(A^t and A^s derived from static failure tests)

$$\sigma^{eff} = \sqrt{A^t\{I^{m,t}\}^2 + I^{m,s1} + A^s I^{m,s2}}$$

$$I^{m,t} = \frac{1}{2}\left[\sigma_{22}^m + \sigma_{33}^m + \sqrt{(\sigma_{22}^m + \sigma_{33}^m)^2 - 4(\sigma_{22}^m\sigma_{33}^m - \sigma_{23}^m)}\right]$$

$$I^{m,s1} = (\sigma_{12}^m)^2 + (\sigma_{13}^m)^2$$

$$I^{m,s2} = \left(\frac{1}{4}(\sigma_{22}^m - \sigma_{33}^m)^2 + (\sigma_{23}^m)^2\right)$$

$$\sigma_{ij}^m = \frac{1}{(1 - v^f)}\left[\delta_{ir}\delta_{js} - C_{ijpq}^f S_{pqrs}^m\right]^{-1}\left[\delta_{rk}\delta_{sl} - C_{rspq}^f S_{pqkl}^c\right]\sigma_{kl}^c$$

*Jensen, E. M. and Fertig, R. S., "Physics-Based Multiscale Creep Strain and Creep Rupture Modeling for Composite Materials," *AIAA Journal,* Vol. 54, No. 2, 2015, pp. 703-711

Case Study: Fatigue Stress Minimization on SWiFT Wind Turbine Blade

The goal was set to minimize the effective off-axis matrix stress derived by Fertig in the SWiFT wind blade model under five loading conditions:

1) Centrifugal loading (static, assuming angular velocity 43 rpm)
2) Gravitational loading (dynamic)
3) Aerodynamic (static, loads generated by NSU3D, inflow = 12 m/s)
4) Combined loading (static, with blade in horizontal position)
5) Combined loading (dynamic, through 3 revolutions)

Case Study: Fatigue Stress Minimization on SWiFT Wind Turbine Blade

Objective function defined as fourth-power p-norm of effective off-axis matrix stress:

$$L = \int_0^t \int_\Omega \left(\sigma^{eff}\right)^4 d\Omega dt$$

A power of four has been observed to target areas of maximum stress, while keeping objective smooth and reasonably well behaved*.

*Duysinx, P. and Sigmund, O., "New Developments in Handling Stress Constraints in Optimal Material Distribution." *Proceedings of the 7th AIAA/USAF/NASA/ISSMO Symposium on Multidisciplinary Analysis and Optimization*, Vol. 1, 1998.

Case Study: Fatigue Stress Minimization on SWiFT Wind Turbine Blade

Design variables: in-plane fiber angle with respect to blade's longitudinal axis assuming single-ply panels. One set with a variable defining angle for each section, and one set with a variable for each individual element of the structure.

$$\alpha_{pq}^{i}(D_i) = \begin{bmatrix} \cos(D_i) & \sin(D_i) & 0 \\ -\sin(D_i) & \cos(D_i) & 0 \\ 0 & 0 & 1 \end{bmatrix}_{pr} \alpha_{rq}^{i,0}$$

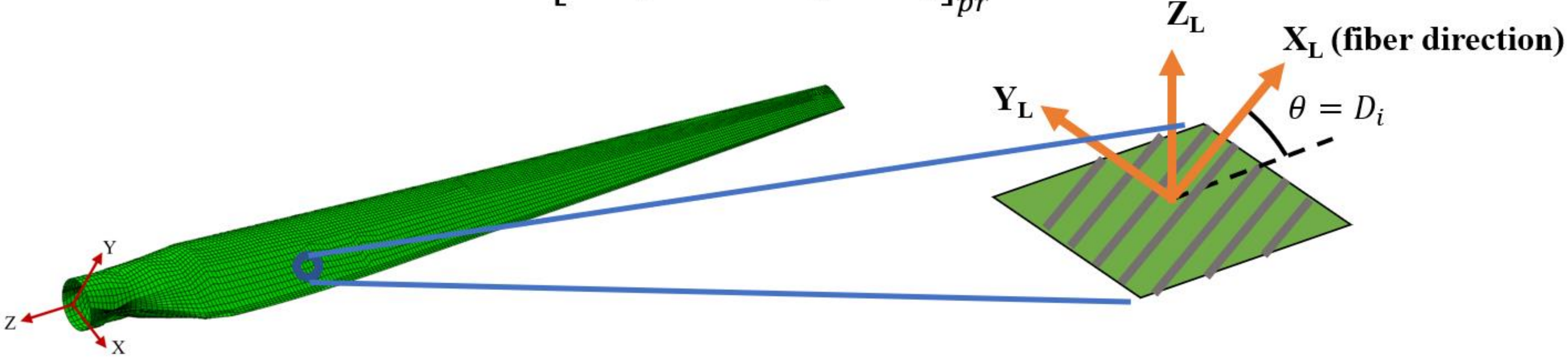

(blade sections)

Case Study: Fatigue Stress Minimization on SWiFT Wind Turbine Blade

Chang in max stress and deflection for all 5 load cases:

Load Case	Section Design Variables: Change in Max Stress	Section Design Variables: Change in Max Deflection	Element Design Variables: Change in Max Stress	Element Design Variables: Change in Max Deflection
Centrifugal	-37.67%	-0.64%	-59.41%	-7.43%
Gravitational	-45.69%	-0.50%	-55.49%	0.12%
Aerodynamic	-18.63%	-0.40%	-42.30%	-2.82%
Combined, Static	-19.24%	0.24%	-54.08%	-6.71%
Combined, Dynamic	-21.72%	0.13%	-51.11%	-9.05%

Case Study: Fatigue Stress Minimization on SWiFT Wind Turbine Blade

Experimental correlation* between effective off-axis matrix stress amplitude and fatigue life:

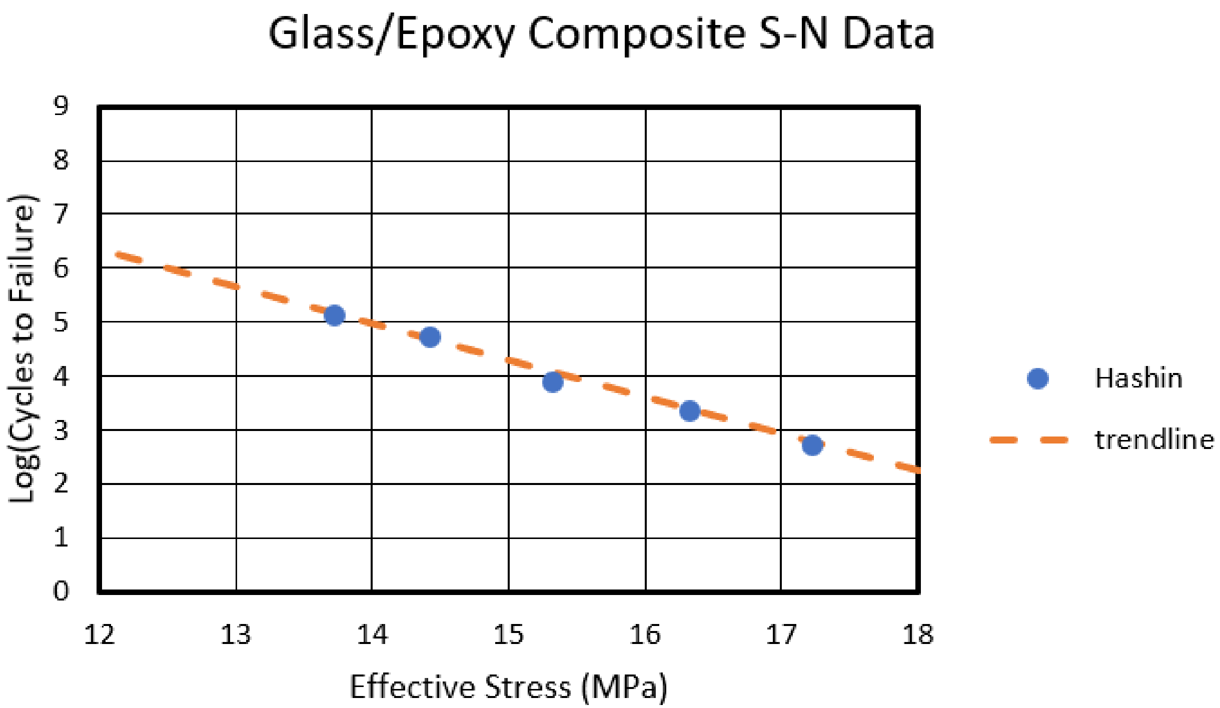

Case Study: Fatigue Stress Minimization on SWiFT Wind Turbine Blade

Optimization history for combined dynamic loading:

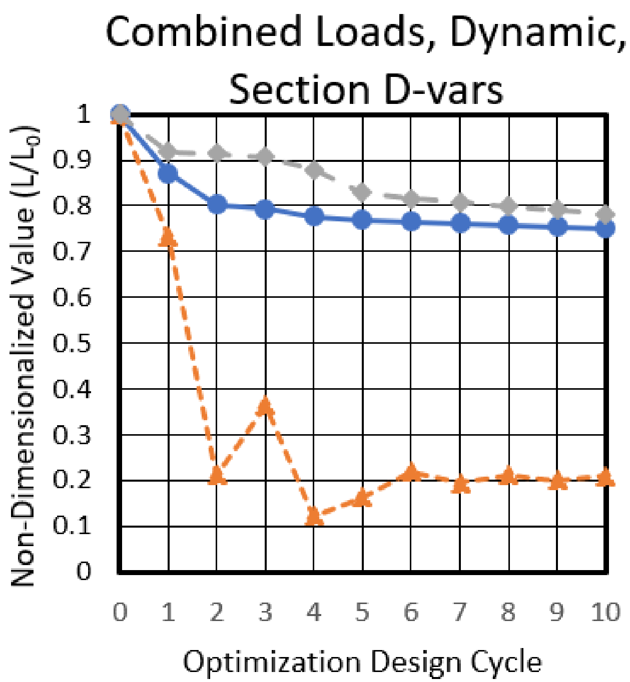

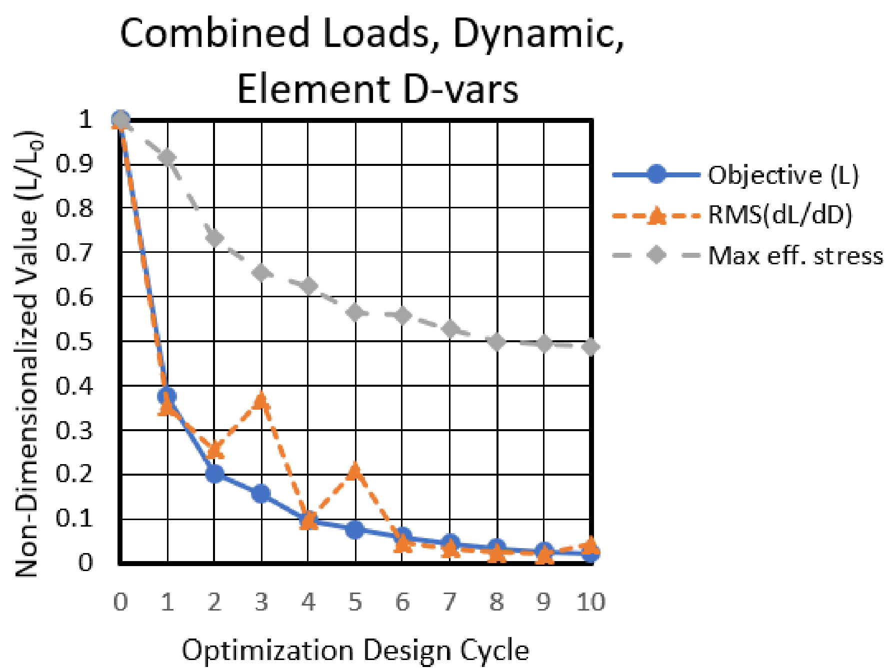

Case Study: Fatigue Stress Minimization on SWiFT Wind Turbine Blade

Fiber angle change for combined dynamic loading:

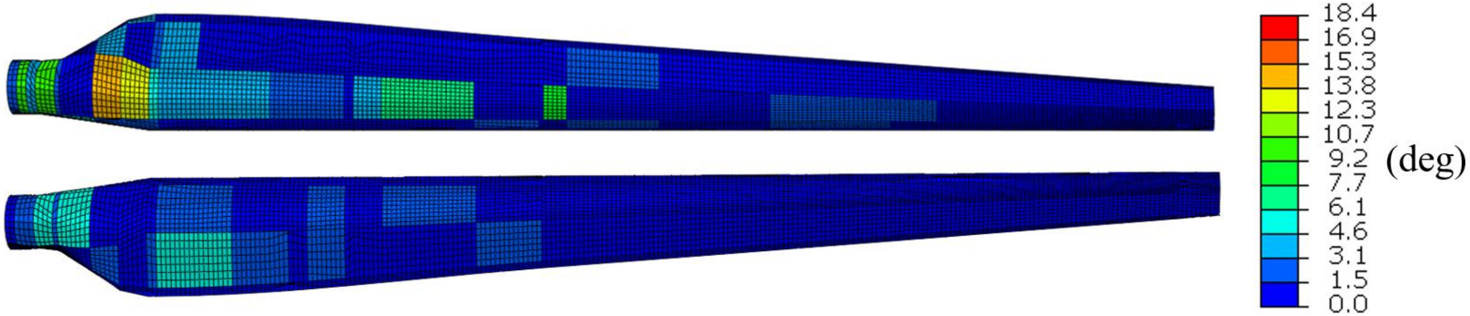

(a) Section design variables

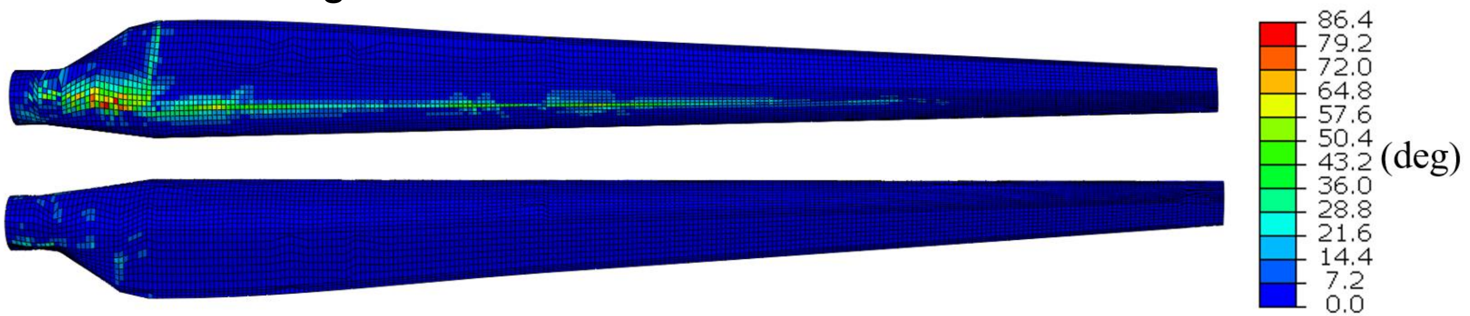

(b) Element design variables

Case Study: Fatigue Stress Minimization on SWiFT Wind Turbine Blade

Stress reduction for combined dynamic loading:

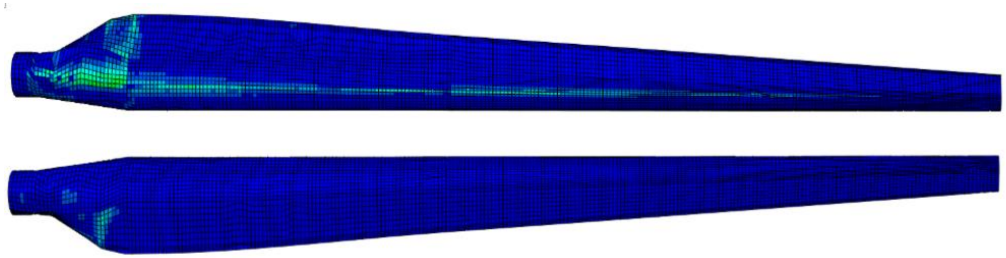

(a) Before optimization

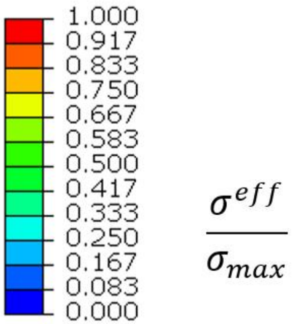

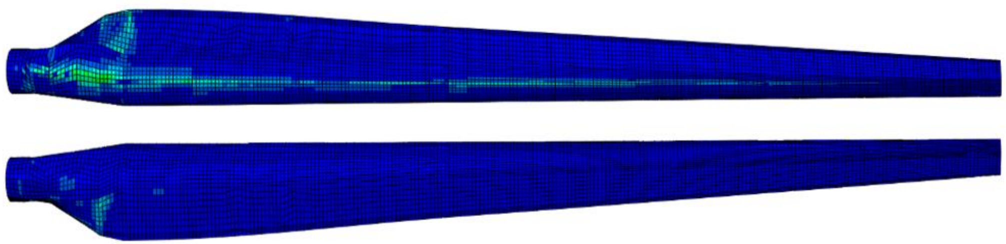

(b) After, section design variables

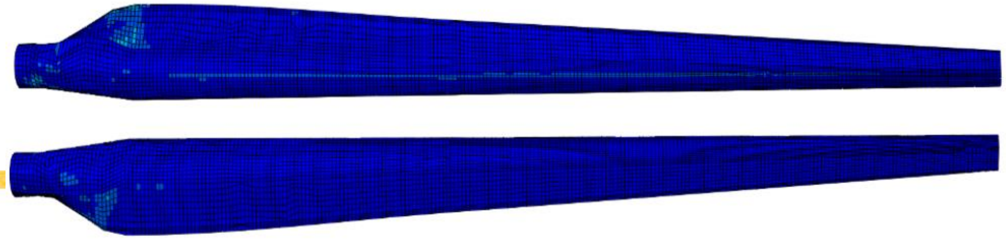

(c) After, element design variables

Case Study: Buckling Constraints on a Truss-Braced Wing

- Current push in aviation toward fuel efficiency through high-aspect ratio wing designs.
- Increased importance to consider buckling in design analysis.

Case Study: Buckling Constraints on a Truss-Braced Wing

Two main common approaches to structural buckling analysis:

1) Approximate structures as collection of simplified members such as beams or flat plates and apply analytical solutions. Computationally inexpensive but generally inaccurate, and can be cumbersome to implement.
2) Generalized eigenmode analysis on nonlinear structural stiffness matrix. Expensive, can be problematic with duplicate eigenvalues, appropriate number of eigenpairs not always intuitive.

A generally applicable and affordable approach suitable for gradient-based optimization would be valuable.

Case Study: Buckling Constraints on a Truss-Braced Wing

Elastic structures subject to conservative forces behave in such a way to minimize total potential energy:

$$\Pi = \int_{\Omega} V d\Omega - \int_{\Omega} f_i u_i d\Omega - \int_{S} t_i u_i dS$$

V = strain energy density

If displacement is a function of a set of discrete parameters, $u_i = N_{ij} U_j$, then state of equilibrium defined by

$$\frac{\partial \Pi}{\partial U_j} = \int_{\Omega} \frac{\partial V}{\partial \epsilon_k} \frac{\partial \epsilon_k}{\partial U_j} d\Omega - \int_{\Omega} f_i N_{ij} d\Omega - \int_{S} t_i N_{ij} dS = 0$$

Case Study: Buckling Constraints on a Truss-Braced Wing

If there exists a mode of displacement $\boldsymbol{\delta U}$ in which continued deformation from equilibrium results in accelerated decrease of total potential energy, the system is in unstable equilibrium. The second-order Taylor series expansion of total potential energy is

$$\delta\Pi = \frac{\partial \Pi}{\partial U_i}\delta U_i + \frac{1}{2}\frac{\partial^2 \Pi}{\partial U_i \partial U_j}\delta U_i \delta U_j$$

Case Study: Buckling Constraints on a Truss-Braced Wing

If there exists a mode of displacement $\boldsymbol{\delta U}$ in which continued deformation from equilibrium results in accelerated decrease of total potential energy, the system is in unstable equilibrium. The second-order Taylor series expansion of total potential energy is

zero at equilibrium

$$\delta\Pi = \cancel{\frac{\partial \Pi}{\partial U_i}\delta U_i} + \frac{1}{2}\frac{\partial^2 \Pi}{\partial U_i \partial U_j}\delta U_i \delta U_j$$

Case Study: Buckling Constraints on a Truss-Braced Wing

The matrix of second-order derivatives of potential energy is

$$\frac{\partial^2 \Pi}{\partial U_i \partial U_j} = \int_\Omega \left(\frac{\partial^2 V}{\partial \epsilon_p \partial \epsilon_k} \frac{\partial \epsilon_p}{\partial U_j} \frac{\partial \epsilon_k}{\partial U_i} + \frac{\partial V}{\partial \epsilon_k} \frac{\partial^2 \epsilon_k}{\partial U_i \partial U_j} \right) d\Omega$$

Or, with the partial derivatives of strain energy density represented as stress and stiffness,

$$\frac{\partial^2 \Pi}{\partial U_i \partial U_j} = \int_\Omega \left(C_{pk} \frac{\partial \epsilon_p}{\partial U_j} \frac{\partial \epsilon_k}{\partial U_i} + \sigma_k \frac{\partial^2 \epsilon_k}{\partial U_i \partial U_j} \right) d\Omega$$

Nonlinear stiffness matrix

Conclusion: A structure is in a stable, buckling-safe state if the nonlinear stiffness matrix is positive definite.

Case Study: Buckling Constraints on a Truss-Braced Wing

Proposed approach:

1) Perform $[L][d][L^T]$ factorization on the nonlinear structural stiffness matrix at a given state.
2) Find a perturbation vector $\delta\boldsymbol{U}$ with back-substitution such that

$$L_{ji}\delta U_j = \begin{cases} d_{ii} \; in \; rows \; where \; d_{ii} < 0 \\ \\ 0 \; in \; rows \; where \; d_{ii} \geq \; 0 \end{cases}$$

3) Let the constraint for structural stability be defined by

$$\lfloor \boldsymbol{\delta U}^T \rfloor [K] \{\boldsymbol{\delta U}\} = 0$$

Case Study: Buckling Constraints on a Truss-Braced Wing

Drawback: No cost-effective way of computing the sensitivity of the matrix factorization. Sensitivity of the scalar buckling criterion must be approximated

$$\frac{d}{dD}(\lfloor \boldsymbol{\delta U}^T \rfloor [K] \{\boldsymbol{\delta U}\}) \approx \lfloor \boldsymbol{\delta U}^T \rfloor \left[\frac{dK}{dD}\right] \{\boldsymbol{\delta U}\}$$

Advantage: Only one matrix factorization and a differentiation of K is required at each design state. Eigenvalue-based approach requires similar operation for *each* eigenpair at each design state.

Goal: Investigate the proposed method, compared to standard eigenvalue-based analysis and assess its feasibility.

Case Study: Buckling Constraints on a Truss-Braced Wing

- Buckling analysis was performed on a flat plate using both LDL buckling criterion and eigenvalue-based criterion.
- Thickness of each of four square sections defined as design variables
- The load P and material properties chosen so that critical buckling thickness = 0.05

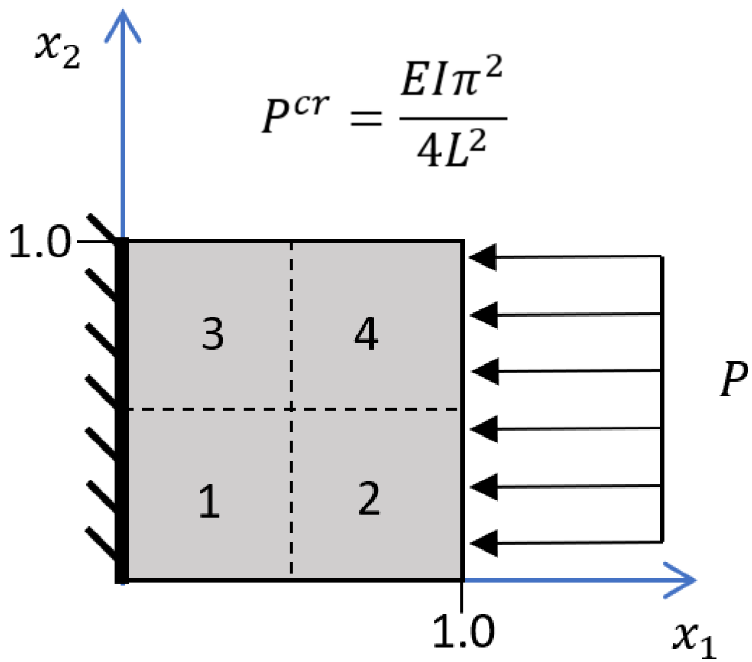

Case Study: Buckling Constraints on a Truss-Braced Wing

Objective set to minimize total volume of the flat plate while ensuring structural stability:

$$L = \sum_{i=1}^{n_{els}} Vol_i - \lfloor \boldsymbol{\delta U}^T \rfloor [K] \{\boldsymbol{\delta U}\}$$ (LDL criterion)

$$L = \sum_{i=1}^{n_{els}} Vol_i + c \sum_{j=1}^{n_{vals}} e^{-2\kappa\lambda_j}$$ (Eigenvalue-based criterion)

Case Study: Buckling Constraints on a Truss-Braced Wing

Sensitivities for LDL criterion at thicknesses below critical:

Section	Sensitivities		Unit Direction	
	Adjoint	Complex	Adjoint	Complex
1	-4.97325E+06	-1.49197E+07	-7.173427412188**40**E-01	-7.173427412188**84**E-01
2	-1.11251E+06	-3.33753E+06	-1.604687353993**71**E-01	-1.604687353993**92**E-01
3	-4.54578E+06	-1.36374E+07	-6.55685295716**613**E-01	-6.55685295716**418**E-01
4	-1.19571E+06	-3.58714E+06	-1.724701990518**47**E-01	-1.724701990518**52**E-01

In this case sensitivity direction is correct, but magnitude off by factor of three (not generally true).

Case Study: Buckling Constraints on a Truss-Braced Wing

Optimization results:

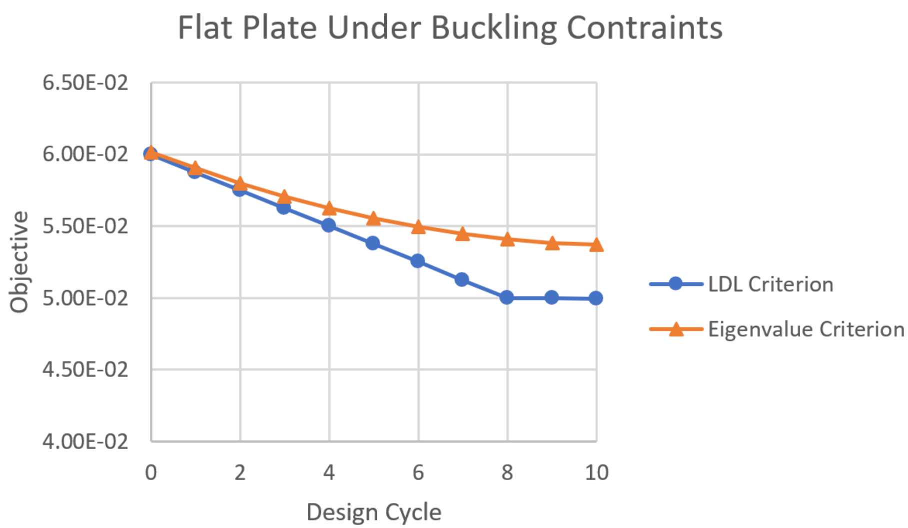

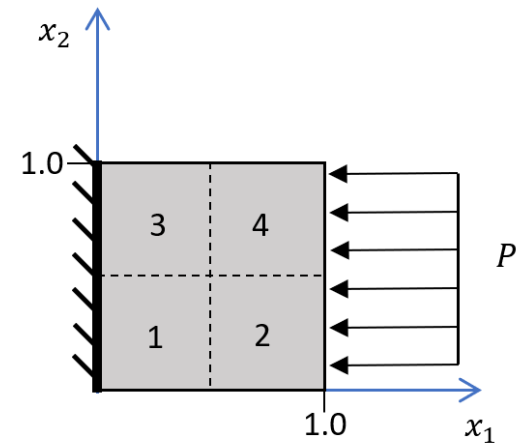

Quantity	LDL Criterion	Eigenvalue Criterion
Sec. 1 thickness	5.0434E-02	5.6537E-02
Sec. 2 thickness	4.8023E-02	4.3509E-02
Sec. 3 thickness	5.0434E-02	5.6537E-02
Sec. 4 thickness	4.8023E-02	4.3509E-02
Total volume	4.9229E-02	5.0023E-02

LDL criterion tends to cause abrupt behavior at point of instability.

Case Study: Buckling Constraints on a Truss-Braced Wing

Truss-Braced wing model:

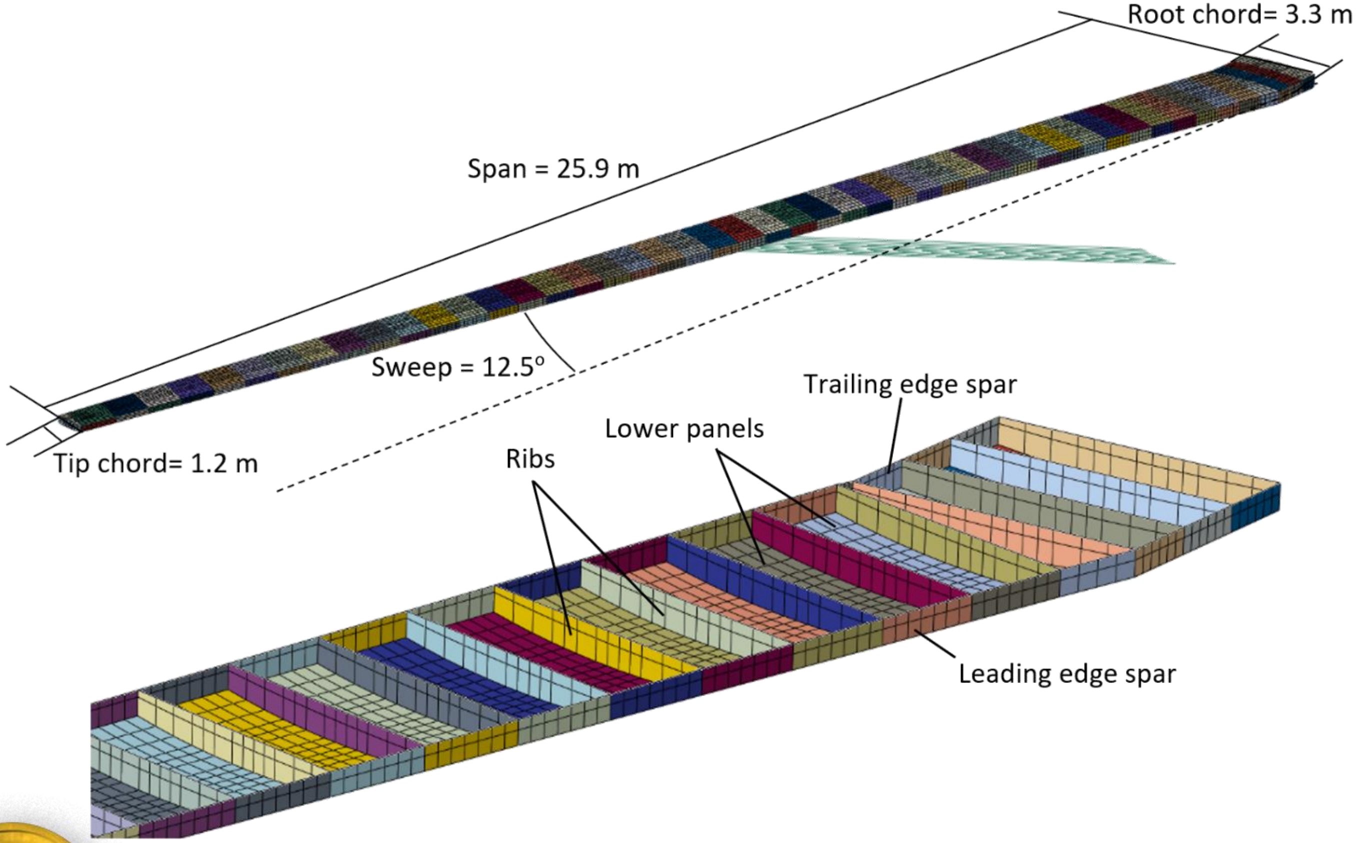

Airfoil: CRM.65*

≈ 12,000 four-node shell elements

Thickness of each panel, rib and spar section defined as design variables

*Vassberg, J.C., DeHaan, M.A., Rivers, S.M., and Wahls, R.A., "Development of a Common Research Model for Applied CFD Validation Studies," *26th AIAA Applied Aerodynamics Conference,* CP2008-6919, 2008.

Case Study: Buckling Constraints on a Truss-Braced Wing

Spanwise elliptic load distribution:

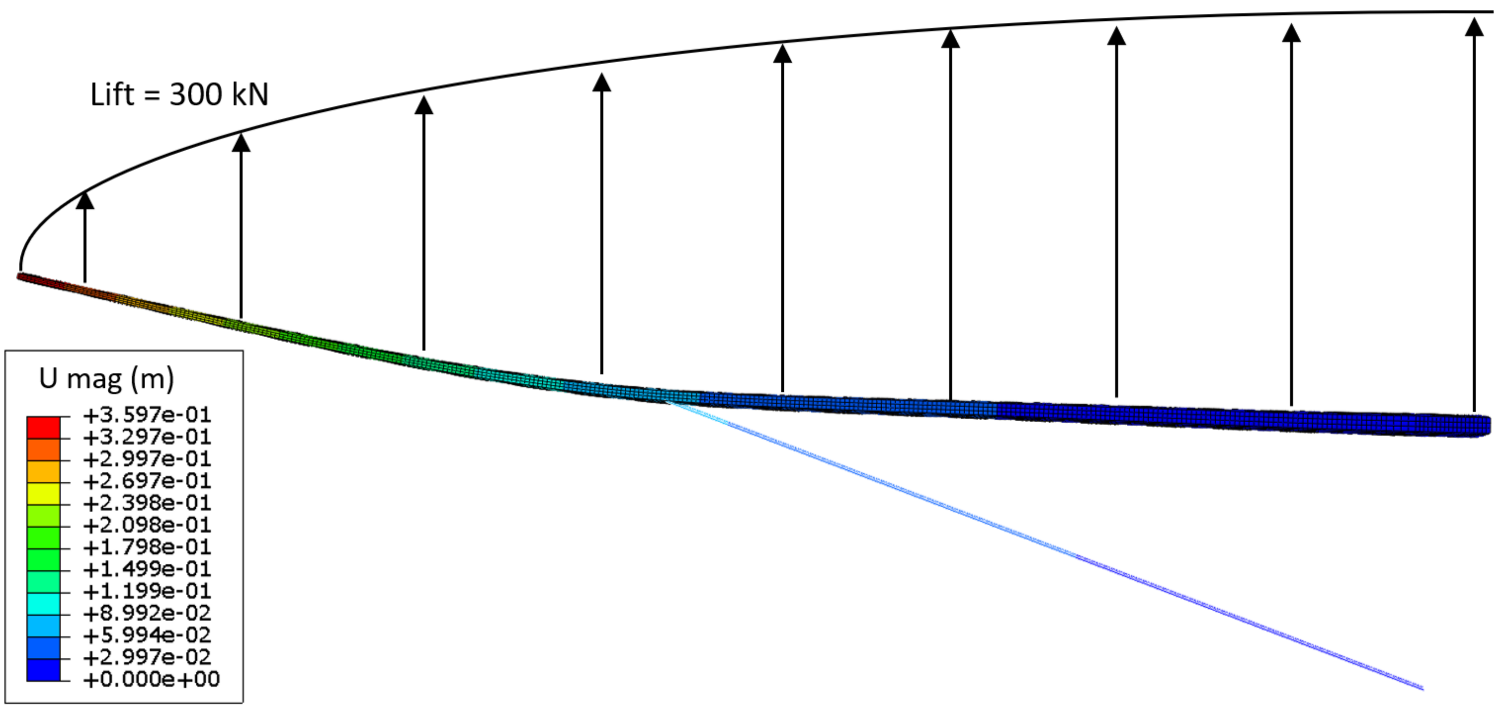

Case Study: Buckling Constraints on a Truss-Braced Wing

Objective set to minimize mass subject to structural stability and mises stress below yield strength for aluminum (using Kreisselmeier–Steinhauser aggregation*):

$$L = \sum_{i=1}^{n_{els}} Vol_i - \lfloor \boldsymbol{\delta U}^T \rfloor [K] \{\boldsymbol{\delta U}\} + h \frac{1}{(Total\,Vol)} \sum_{k=1}^{n_{els}} e^{2\left(\frac{\sigma_k^v}{\sigma^m}\right)} Vol_k$$ (LDL criterion)

$$L = \sum_{i=1}^{n_{els}} Vol_i + c \sum_{j=1}^{n_{vals}} e^{-2\kappa\lambda_j} + h \frac{1}{(Total\,Vol)} \sum_{k=1}^{n_{els}} e^{2\left(\frac{\sigma_k^v}{\sigma^m}\right)} Vol_k$$ (Eigenvalue criterion)

*Kreisselmeier G., Steinhauser R., “Systematic Control Design by Optimizing a Vector Performance Indicator,” *Symposium on Computer-Aided Design of Control Systems*, IFAC, Zurich, Switzerland, 1979 pp. 113–117.

Case Study: Buckling Constraints on a Truss-Braced Wing

Sensitivities for LDL criterion:

	Sensitivities		Unit Direction	
Section	Adjoint	Complex	Adjoint	Complex
1	5.8177E+24	3.6156E+26	8.3054E-01	7.6316E-01
2	3.3838E+24	2.3923E+26	4.8308E-01	5.0496E-01
3	1.7267E+24	1.5660E+26	2.4650E-01	3.3055E-01
4	5.5874E+23	6.6266E+25	7.9766E-02	1.3987E-01
5	6.9036E+23	8.7057E+25	9.8557E-02	1.8376E-01

Angle of difference = 8.68^{o}

Case Study: Buckling Constraints on a Truss-Braced Wing

Optimization results:

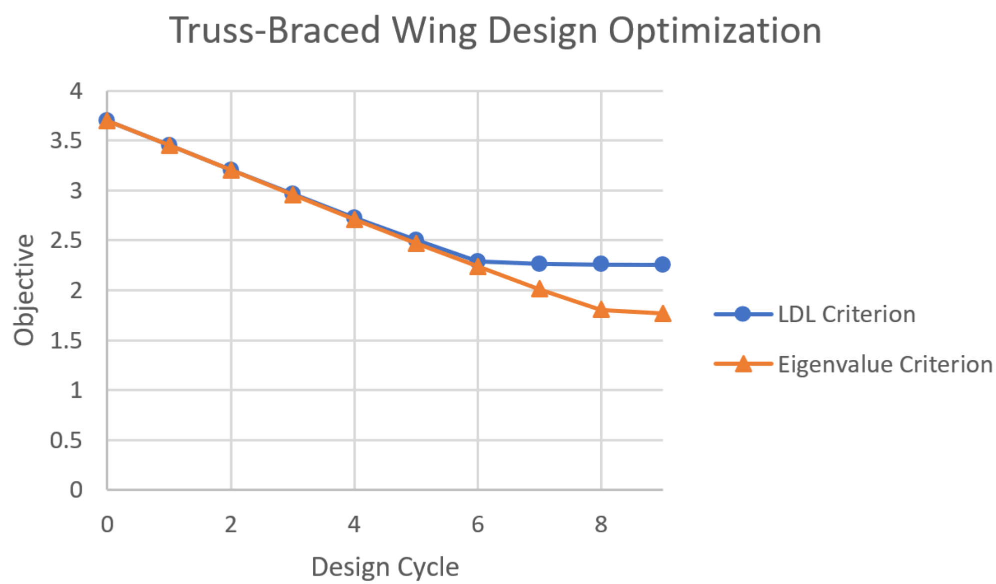

Again abrupt convergence is seen at the point of constraint violation, especially for LDL criterion.

Case Study: Buckling Constraints on a Truss-Braced Wing

Final panel thickness distribution:

Initial mass = 8500 kg

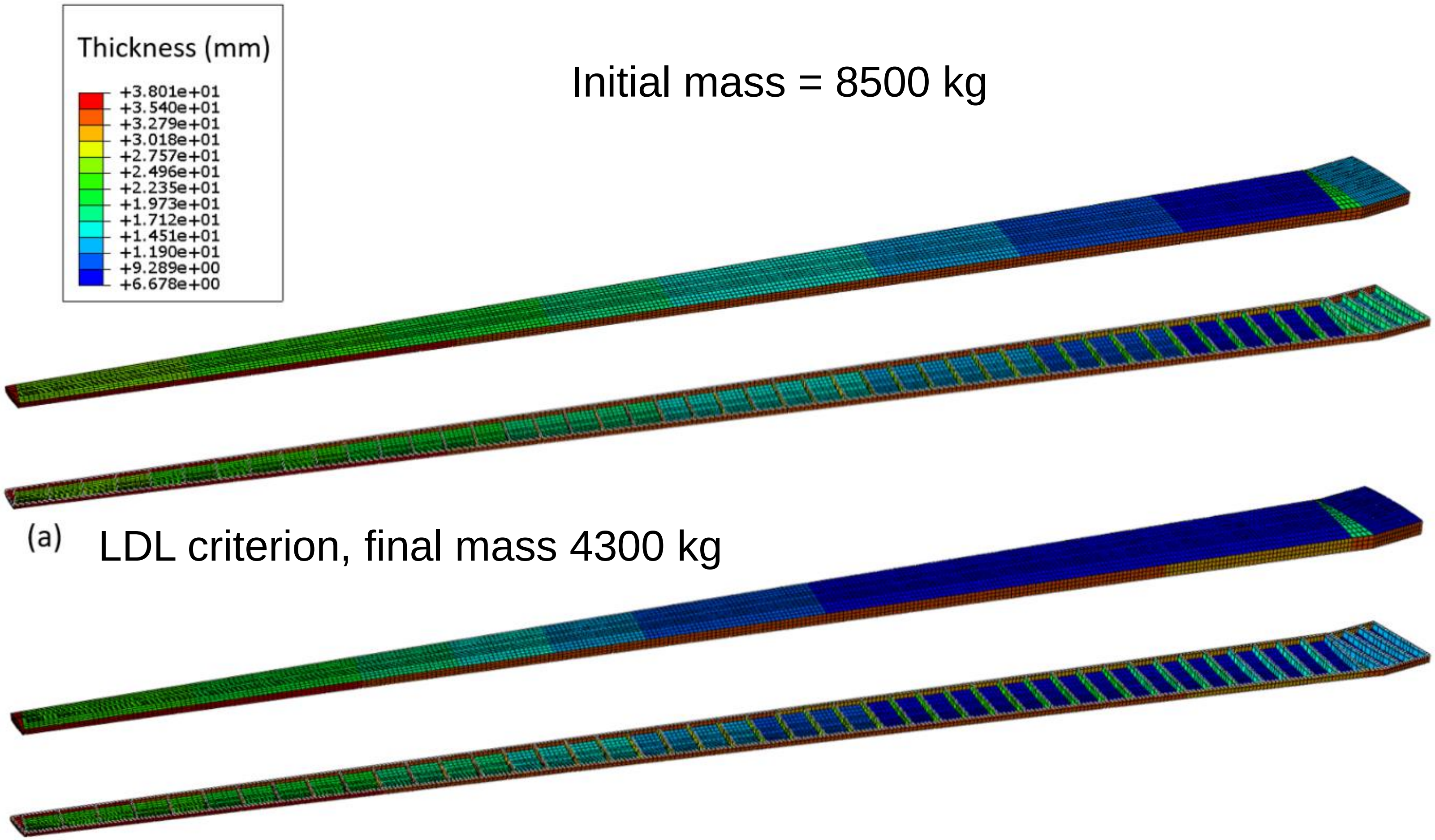

(a) LDL criterion, final mass 4300 kg

(b) Eigenvalue criterion, final mass 3400 kg

Conclusions

- AStrO has been developed and validated as a reliable tool for structural thermoelastic modeling and sensitivity analysis.
- Highly specialized and novel investigations have been made possible by the open-source nature of the package.
- There may be great potential to improve fatigue life in composite structures through fiber angle optimization, but results are highly dependent on loading and fully coupled aeroelastic optimization should yield the best results.
- The proposed LDL criterion for buckling constraints is an effective and computationally efficient metric for enforcing structural stability. Further investigations required to understand limitations and the best implementation.

Future Work

- Completion of all tools for fully coupled aeroelastic optimization would make it possible to conduct further meaningful studies to enrich what has been done.
- Parallelization of AStrO would enable more in-depth studies of generalized buckling analysis and other topics.
- Continue studies with more sophisticated optimizers.
- Extension of AStrO's tools to account for nonlinearity in thermal material properties for investigations in hypersonic applications.
- Possible applications in high-speed ballistic dynamics may require alternative time-integration schemes.

Publications

1. Anderson, E., Bhuiyan, F., Mavriplis, D., and Fertig, R., “Adjoint-Based High-Fidelity Structural Optimization of Wind Turbine Blade for Load Stress Minimization,” *AIAA Journal, (in pending)*
2. Anderson, E., Bhuiyan, F., Mavriplis, D., and Fertig, R., “Adjoint-Based High-Fidelity Aeroelastic Optimization of Wind Turbine Blade for Load Stress Minimization,” *AIAA 2018 Wind Energy Symposium,* CP18-1241.
3. Marviplis, D., Fabiano, E., and Anderson, E., “Recent Advances in High-Fidelity Multidisciplinary Adjoint-Based Optimization with the NSU3D Flow Solver Framework,” *55th AIAA Aerospace Sciences Meeting,* CP17-1669, 2017.
4. Mavriplis, D., Anderson, E., Fertig, R. S., and Garnich, M., “Development of a High-Fidelity Time-Dependent Aero-Structural Capability for Analysis and Design,” *57th AIAA/ASCE/AHS/ASC Structures, Structural Dynamics, and Materials Conference,* CP1175, 2016.
5. Garnich, M., Fertig, R., and Anderson, E., “Random Fiber Micromechanics of Fatigue Damage,” *54th AIAA/ASME/ASCE/AHS/ASC Structures, Structural Dynamics, and Materials Conference,* CP1656, 2013.

Acknowledgements

- Funding Sources:
  - U.S. Department of Energy, Office of Science, Basic Energy Sciences, under Award DE-SC0012671
  - NASA University Leadership Initiative (ULI) program, 2017 award for development of ultra-efficient commercial vehicles
  - University of Wyoming's College of Engineering and Applied Sciences Energy Graduate Assistantship
- Committee: Dimitri Mavriplis, Ray Fertig III, Yang Liu, Victor Ginting, Mark Garnich, Richard Schmidt
- My wife and my family for their support and for keeping me going.

UNIVERSITY OF WYOMING

Thank you

Questions?

AStrO: Adjoint-Based Structural Optimizer

Demonstration: Nonlinear deflection of clamped bar subject to constant moment, forming a circular ring.

	Coarse Mesh	Medium Mesh	Fine Mesh
RMS(error)	1.26655	0.623806	0.334779

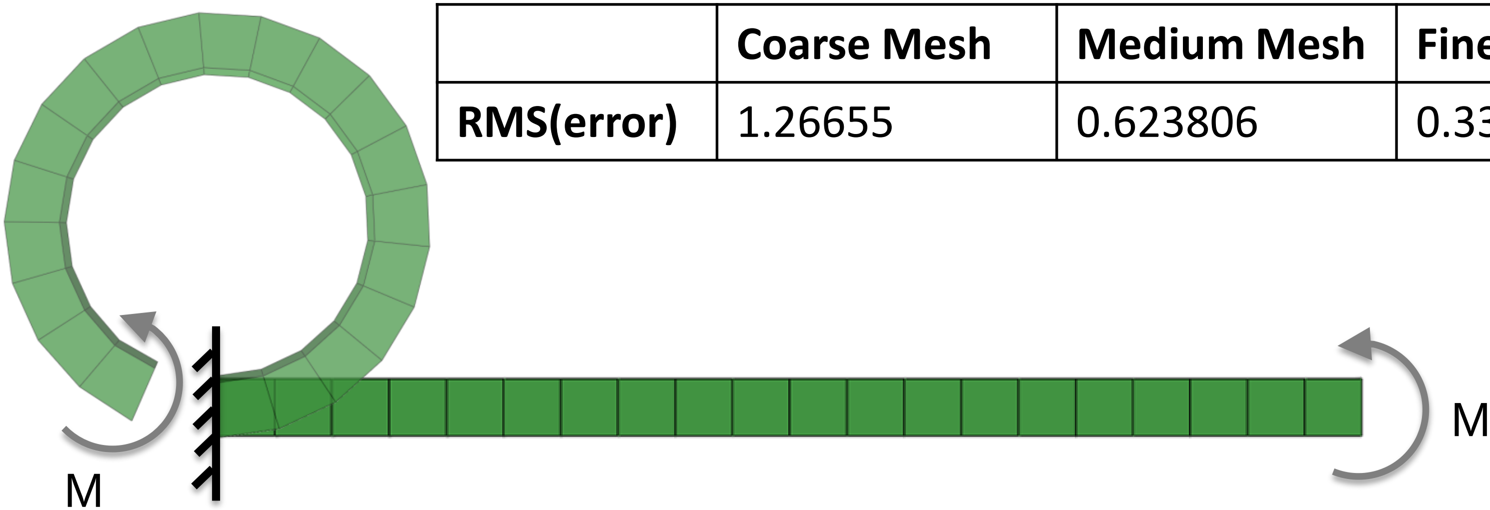

AStrO: Adjoint-Based Structural Optimizer

Demonstration: Critical buckling load of square flat plate subject to uniform bi-axial loading

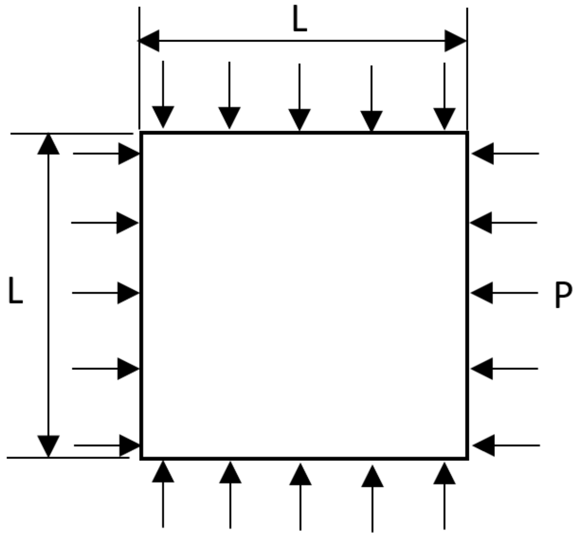

	Analytical	Coarse Mesh	Medium Mesh	Fine Mesh
Critical Load	1.66155	1.72342	1.67157	1.65547
% Error		3.7236%	0.6031%	0.3659%

Eigenpair-based objectives

$$[K]\boldsymbol{v}_i = \lambda_i \boldsymbol{v}_i$$

$$L = L(\boldsymbol{v}_i, \lambda_i)$$

$$\frac{d[K]}{dD_j}\boldsymbol{v}_i + [K]\frac{d\boldsymbol{v}_i}{dD_j} = \frac{d\lambda_i}{dD_j}\boldsymbol{v}_i + \lambda_i \frac{d\boldsymbol{v}_i}{dD_j}$$

$$\frac{dL}{dD_j} = \frac{\partial L}{\partial \boldsymbol{v}_i}\frac{d\boldsymbol{v}_i}{dD_j} + \frac{\partial L}{\partial \lambda_i}\frac{d\lambda_i}{dD_j}$$

$$\boldsymbol{v}_i^T \boldsymbol{v}_i = 1$$

$$\Rightarrow \boldsymbol{v}_i^T \frac{d\boldsymbol{v}_i}{dD_j} = 0$$

$$\begin{bmatrix} [K] - \lambda_i[I] & -\boldsymbol{v}_i \\ -\boldsymbol{v}_i^T & 0 \end{bmatrix} \begin{Bmatrix} \dfrac{d\boldsymbol{v}_i}{dD_j} \\ \dfrac{d\lambda_i}{dD_j} \end{Bmatrix} = \begin{Bmatrix} -\dfrac{d[K]}{dD_j}\boldsymbol{v}_i \\ 0 \end{Bmatrix}$$

Eigenpair-based objectives

$$\frac{dL}{dD_j} = \begin{bmatrix} \frac{\partial L}{\partial \boldsymbol{v}_i^T} & \frac{\partial L}{\partial \lambda_i} \end{bmatrix} \begin{Bmatrix} \frac{d\boldsymbol{v}_i}{dD_j} \\ \frac{d\lambda_i}{dD_j} \end{Bmatrix} = \begin{bmatrix} \frac{\partial L}{\partial \boldsymbol{v}_i^T} & \frac{\partial L}{\partial \lambda_i} \end{bmatrix} \begin{bmatrix} [K] - \lambda_i[I] & -\boldsymbol{v}_i \\ -\boldsymbol{v}_i^T & 0 \end{bmatrix}^{-1} \begin{Bmatrix} -\frac{d[K]}{dD_j}\boldsymbol{v}_i \\ 0 \end{Bmatrix}$$

$$\frac{d[K]}{dD_j} = \frac{\partial [K]}{\partial D_j} + \frac{\partial [K]}{\partial U_k}\frac{\partial U_k}{\partial R_m}\frac{\partial R_m}{\partial D_j} = \frac{\partial [K]}{\partial D_j} + \frac{\partial [K]}{\partial U_k}\left[\frac{\partial \boldsymbol{R}}{\partial \boldsymbol{U}}\right]_{km}^{-1}\frac{\partial R_m}{\partial D_j}$$

Eigenpair-based objectives

$(1)\ find\ the\ necessary\ eigenpairs\ of\ [K]\colon \lambda_i, \boldsymbol{v}_i$

$(2)\ for\ every\ eigenpair\colon$

$$(a)\ solve \begin{bmatrix} [K]-\lambda_i[I] & -\boldsymbol{v}_i \\ -\boldsymbol{v}_i^T & 0 \end{bmatrix}^T \begin{Bmatrix} \boldsymbol{\Lambda}^v \\ \boldsymbol{\Lambda}^\lambda \end{Bmatrix} = \begin{Bmatrix} \dfrac{\partial L}{\partial \boldsymbol{v}_i^T} \\ \dfrac{\partial L}{\partial \lambda_i} \end{Bmatrix}$$

$$(b)\ evaluate\ y_k = (\boldsymbol{\Lambda}^v)^T \frac{\partial [K]}{\partial U_k} \boldsymbol{v}_i$$

$$(c)\ solve\ \left[\frac{\partial \boldsymbol{R}}{\partial \boldsymbol{U}}\right]_{km}^T \Lambda_m = y_k$$

$$(d)\ for\ every\ D_j\ update \frac{dL}{dD_j} = \frac{dL}{dD_j} - (\boldsymbol{\Lambda}^v)^T \frac{\partial [K]}{\partial D_j} \boldsymbol{v}_i - \boldsymbol{\Lambda}^T \frac{\partial \boldsymbol{R}}{\partial D_j}$$